New Energy Materials and Devices
https://www.sciltp.com/journals/nemd

Review

Synergistic Strategies for Extreme Fast-Charging Lithium-Ion Batteries: Graphite Anode, Electrolyte, and Electrode Architectural Engineering

Qihang Ding [1], Hui Li [2,*] and Xinping Ai [1,*]

[1] Hubei Key Laboratory of Electrochemical Power Sources, College of Chemistry & Molecular Sciences, Wuhan University, Wuhan 430072, China
[2] State Key Laboratory of New Textile Materials and Advanced Processing, Wuhan Textile University, Wuhan 430200, China
* Correspondence: lih@whu.edu.cn (H.L.); xpai@whu.edu.cn (X.A.)

How To Cite: Ding, Q.; Li, H.; Ai, X. Synergistic Strategies for Extreme Fast-Charging Lithium-Ion Batteries: Graphite Anode, Electrolyte, and Electrode Architectural Engineering. *New Energy Materials and Devices* **2026**, *1*(1), 10–33.

Received: 13 April 2026
Revised: 8 May 2026
Accepted: 29 May 2026
Published: 16 June 2026

Abstract: Extreme fast charging (XFC) of lithium-ion batteries (LIBs) is essential for alleviating charging anxiety and accelerating electric vehicles adoption, but it remains challenging due to lithium plating on graphite anodes under high-rate conditions. This review systematically summarizes recent advances and synergistic strategies for achieving XFC from three integrated perspectives: graphite anodes, electrolytes, and electrode architectures. The fundamental limitations leading to lithium plating are first analyzed, including the high desolvation energy barrier as the rate-determining step, the anisotropic nature of graphite that restricts active intercalation sites, and the polarization heterogeneity along the thickness of porous electrodes. For graphite anodes, strategies such as etching-induced porosity, edge-plane functionalization, heterostructure construction, and artificial SEI engineering are discussed to increase active-site density and lower the desolvation barrier. In electrolyte design, the focus has shifted from maximizing ionic conductivity alone to synergistically enhancing Li^+ transport and interfacial kinetics. Representative approaches include low-viscosity co-solvents, highly dissociative lithium salts, weakly coordinating solvents, localized high-concentration electrolytes, bulky-anion or polyanionic electrolytes, and low-desolvation-energy solvents. For electrode architectures, porosity gradients and low-tortuosity designs are highlighted to facilitate Li^+ transport while preserving energy density. Finally, key future directions are proposed, including multi-objective optimization, quantitative modeling, emerging materials, and degradation management. This review provides a comprehensive framework for the rational design of fast-charging LIBs through coordinated engineering across materials, electrolytes, and electrode structures.

Keywords: extreme fast-charging; lithium-ion batteries; graphite anode; electrolyte design; electrode architectures

1. Introduction

Escalating environmental challenges and the pursuit of sustainable societal development are accelerating the global energy transition toward renewable sources, including wind and solar power [1,2]. In this context, electric vehicles (EVs) are of great strategic importance as a key enabler for integrating renewable energy at scale and building a clean, efficient new energy system [3–5]. Nevertheless, the widespread commercialization of EVs hinges not only on their life-cycle environmental benefits, but, more critically, on two user-centric metrics: driving range and energy replenishment efficiency [6–8]. The driving range determines the vehicle's operational radius,

while the charging rate governs refueling convenience and emergency usability. Collectively, these two parameters constitute the key technological pillars influencing consumer adoption and large-scale market penetration [9–11].

In recent years, continuous advances in LIB chemistries, combined with progress in system-level integration technologies, such as cell-to-pack (CTP) architectures without discrete module, have enabled electric vehicles to routinely achieve driving ranges exceeding 600 km, with high-end models surpassing 700 km under practical operating conditions. Consequently, the so-called "range anxiety" has been substantially mitigated (Figure 1a) [10,12]. However, unlike internal combustion engine vehicles, where refueling can be completed within minutes, even the fastest commercially available fast-charging technologies typically require more than 20 min to charge a battery from a low state of charge (SOC) to 80% SOC [13–15]. This pronounced temporal disparity constitutes the most significant remaining barrier in the transition from combustion-powered vehicles to EVs, often referred to as "charging anxiety," and limits their competitiveness in high-utilization scenarios such as long-distance travel and commercial fleet operations [16]. Accordingly, advancing the extreme fast-charging (XFC) capability of LIBs to match the refueling convenience of gasoline vehicles has emerged as a central research frontier and a strategic priority for both academia and industry [17,18].The United States Advanced Battery Consortium (USABC) has explicitly defined the XFC target as reaching 80% SOC within 10–15 min, corresponding to charge rates of approximately 4C–6C or higher (Figure 1b) [19].

Achieving the XFC target is not merely a matter of increasing the applied charging current; rather, it involves multifaceted scientific and engineering challenges spanning electrochemistry, materials science, thermal management, and system-level optimization. The primary bottleneck, however, lies at the negative electrode, particularly the graphite anode [20–25]. Graphite has been the anode material choice for commercial LIBs over the past three decades owing to its low cost, long cycle life, natural abundance, and well-defined lithium intercalation potential. Nevertheless, its intrinsic physicochemical properties impose pronounced limitations under high-rate charging conditions. First, the lithium intercalation potential of graphite (~0.1 V vs. Li^+/Li) lies in close proximity to the lithium plating potential (0 V vs. Li^+/Li) [26]. Under fast-charging conditions, the combined effects of ohmic, charge-transfer and concentration polarization can lower the local interfacial potential of the graphite anode below 0 V (vs. Li^+/Li), thereby inducing parasitic lithium deposition. The deposited metallic lithium not only reacts chemically with the electrolyte, leading to irreversible consumption of cyclable lithium and electrolyte components, but may also grow into dendritic structures capable of penetrating the separator and causing internal short circuits, posing severe safety risks. Second, graphite exhibits a highly anisotropic structure. The basal planes possess a substantial energy barrier for Li^+ intercalation and are therefore largely electrochemically inactive, whereas lithium insertion predominantly occurs at edge planes that serve as active entry sites [27]. This structural constraint severely limits the effective reaction interface under high-rate conditions, resulting in locally elevated current densities that exacerbate polarization and increase the propensity for lithium plating. Moreover, to enhance cell-level energy density, thick electrodes with high areal loading and low porosity have become increasingly prevalent. Under fast-charging operation, such architectures promote pronounced reaction heterogeneity along the electrode thickness direction, manifesting as preferential lithium plating near the electrode surface in contact with the separator, while the interior graphite remains underutilized. This is a phenomenon widely known as electrode polarization heterogeneity [28]. Finally, the fast-charging performance of graphite anodes is governed by a complex interplay of interfacial and transport processes, including the ionic conductivity of the solid electrolyte interphase (SEI), lithium-ion transport properties in the electrolyte (ionic conductivity, Li^+ transference number, and chemical diffusion coefficient), and the desolvation kinetics of Li^+ at the electrode-electrolyte interface. Kinetic limitations at any of these steps can become rate-determining under XFC conditions, collectively constraining the attainable charging rate.

To address the aforementioned challenges, recent research on fast-charging LIBs has progressed along three synergistic directions: (1) bulk and interfacial modification of graphite anodes, (2) regulation of electrolyte transport and interfacial properties, and (3) rational engineering of electrode architectures. At the anode level, strategies such as pore creation via etching, edge-site functionalization, heterostructure construction, and artificial SEI engineering have been extensively explored. These approaches aim to increase the density of active sites, broaden Li^+ diffusion pathways, lower the energy barrier for lithium intercalation, and accelerate the desolvation process, thereby enhancing the high-rate capability and lithium plating resistance of graphite anodes [29–33]. From the electrolyte perspective, novel electrolyte systems featuring high ionic conductivity, high Li^+ transference number, high diffusion coefficient, and low desolvation energy are being developed through the design of novel lithium salts, solvent optimization, and functional additives, aiming to mitigate polarization, improve mass transport, and strengthen interfacial charge-transfer kinetics [19,34–36]. At the electrode structural level, research has centered on reconciling the intrinsic trade-off between ionic transport kinetics and energy density. By constructing electrodes with gradient porosity, reduced tortuosity, and optimized pore networks, Li^+ transport

along the electrode thickness direction can be facilitated, enabling more homogeneous utilization of active materials under high-rate charging conditions [37–39]. In addition, thermal management, charging protocols, and battery management systems (BMS) have also gradually progressed with the advancement of fast charging. They have respectively undergone paradigm shifts from passive thermal protection to active thermal control, from fixed protocols to intelligent optimization, and from local management to cloud-based collaboration [40–42].

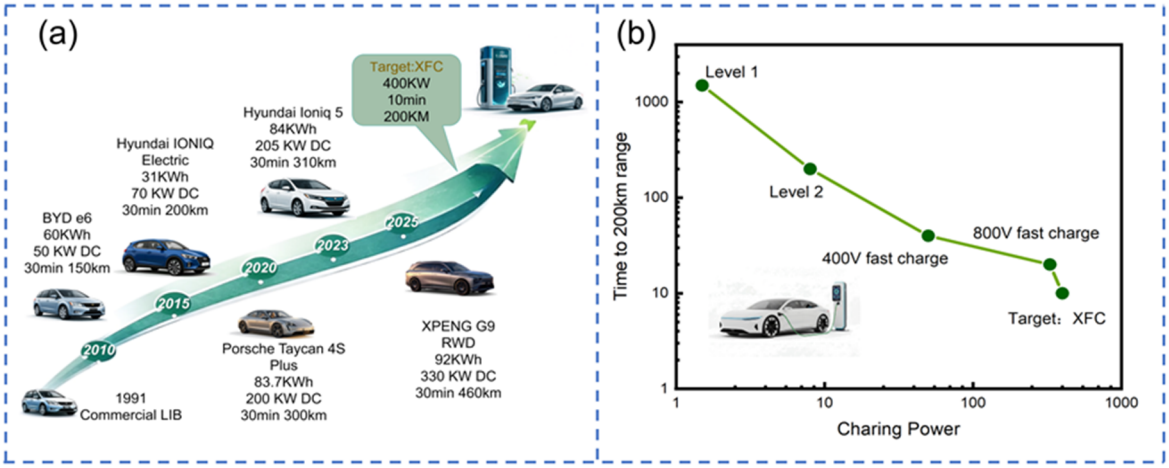

Figure 1. Requirements and development targets for fast-charging LIBs: (**a**) Historical evolution of driving range and charging time for electric vehicles; (**b**) Development target for extreme fast charging (XFC): achieving 80% state of charge (SOC) within 10–15 min.

Despite the substantial progress achieved along these individual directions, how to synergize and integrate various breakthrough strategies to systematically address lithium plating during fast charging, while achieving the XFC target without compromising high energy density, long cycle life, and high safety, remains a major challenge. This Review aims to provide a comprehensive and critical assessment of recent advances in fast-charging LIBs. We first dissect the fundamental mechanisms governing fast-charging performance and lithium plating behavior from three complementary perspectives: electrode reaction kinetics, the intrinsic structural characteristics of graphite anodes, and the reaction heterogeneity inherent to porous electrode architectures. Subsequently, recent progress is summarized in active-site engineering of graphite anodes, electrolyte design and interfacial chemistry regulation, and electrode structural optimization, highlighting representative strategies, prototypical systems, and notable performance breakthroughs. Finally, in light of the current state of the art, we outline future research directions and key technological pathways are outlined, with the objective of providing a coherent theoretical framework and practical guidance for advancing extreme fast-charging LIBs.

2. Key Factors Affecting Fast Charging

The key to enabling fast charging in LIBs is suppressing lithium plating at the anode surface; therefore, identifying the governing factors is of paramount importance. Herein, we systematically analyze the origin and regulation mechanisms of lithium plating from three complementary perspectives: electrode reaction kinetics, intrinsic structural characteristics of graphite anodes, and porous electrode reaction heterogeneity.

2.1. Electrode Reaction Kinetics During Charging

During LIB charging, Li^+ ions are extracted from the cathode and ultimately intercalated into the graphite anode via a multistep pathway (Figure 2a): (1) deintercalation from the cathode lattice, followed by solid-state diffusion to the cathode-electrolyte interphase (CEI); (2) migration across the CEI layer; (3) solvation with solvent molecules in the electrolyte to form solvated Li^+ species; (4) liquid-phase transport of solvated Li^+ to the graphite particle surface; (5) desolvation at the anode/electrolyte interface and permeation into SEI; (6) diffusion across the SEI layer coupled with interfacial charge transfer at the graphite surface; (7) solid-state diffusion within the graphite layers to the final intercalation sites.

To identify the rate-determining step in the charging process, we analyzed the activation energy of each elementary step. As shown in Figure 2b, the activation energy for liquid-phase transport of solvated Li^+ is approximately 10–20 kJ mol^{-1}, whereas that for the desolvation is significantly higher, reaching 50–70 kJ mol^{-1}.

The SEI is typically nanoscale in thickness; consequently, Li^+ diffusion through it imposes only minor resistance and is rarely rate-limiting. The activation energy for interfacial electron transfer at the graphite surface is ~30 kJ mol^{-1}, and that for Li^+ diffusion within the graphite interlayers is about 15–20 kJ mol^{-1} [43,44]. Thus, the desolvation step, possessing the highest activation energy barrier, becomes the rate-determining step in fast charging. This implies that the desolvation process contributes most to interfacial reaction polarization at the graphite anode. Accordingly, reducing the desolvation energy of Li^+ is a critical strategy for improving fast-charging performance.

Temperature exerts a notable influence on the Li^+ desolvation kinetics at the electrode/electrolyte interface. At elevated temperatures, the intensified thermal motion of solvent molecules weakens the Li^+-solvent coordination, thereby effectively reducing the desolvation energy barrier and accelerating the desolvation process. However, excessively high temperatures may simultaneously exacerbate detrimental side reactions such as electrolyte decomposition, compromising the long-term stability of the battery [41].

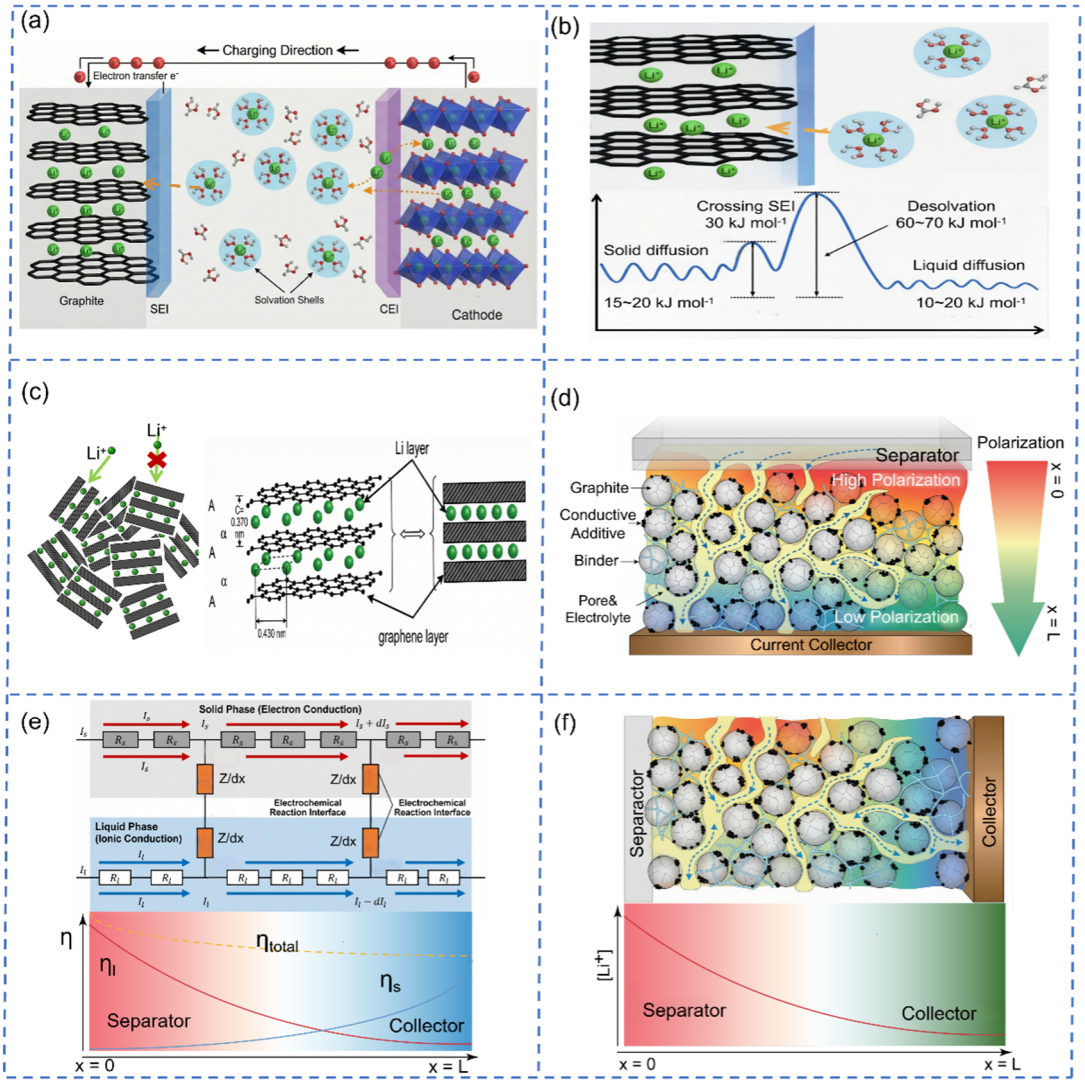

Figure 2. Analysis of factors influencing the fast-charging performance of LIBs: (**a**) Reaction steps during the LIB charging process; (**b**) Activation energies of each elementary step at the graphite anode; (**c**) Schematic of active sites on the graphite anode surface; (**d**) Porous electrode structure and the heterogeneity of reaction and polarization distribution; (**e**) Equivalent circuit of a porous electrode and the distribution of ohmic polarization; (**f**) Lithium-ion concentration distribution along the through-plane direction of the graphite anode at different charging time and rates.

2.2. Structural Characteristics of the Graphite Anode

The structural characteristics of the graphite anode directly govern its fast-charging performance and susceptibility to lithium plating. As a typical intercalation-type anode, interfacial reactions on graphite occur exclusively at active sites where electrons, Li^+ ions, and surface vacancies coexist. A site containing Li^+ and

electrons but lacking available surface vacancies (i.e., the "entry points" for Li^+ intercalation), cannot support effective intercalation. However, graphite exhibits pronounced structural anisotropy. The basal planes present an extremely high energy barrier for Li^+ intercalation (~965 kJ mol^{-1}), making intercalation kinetically impossible. In contrast, the edge plane has a much lower barrier (~29 kJ mol^{-1}) and thus serve as the primary intercalation pathway (Figure 2c) [45,46]. This intrinsic anisotropy severely limits the density of electrochemically active sites, offering only a restricted number of Li^+ entry channels. Furthermore, adjacent graphite layers are held together mainly by van der Waals forces. Under fast intercalation conditions, steep Li^+ concentration gradients between the particle surface and interior generate non-uniform stress distributions, which may induce structural degradation or even mechanical failure. Collectively, the scarcity of active surface sites during high-rate charging leads to elevated local current densities, increased interfacial impedance, and aggravated polarization, thereby promoting lithium plating. Concurrently, the limited interlayer spacing makes the graphite structure vulnerable to degradation upon rapid lithiation/delithiation, contributing to capacity fading and further exacerbating the risk of lithium deposition under XFC conditions.

2.3. Reaction Characteristics of Porous Electrodes

Similar to most electrochemical energy storage systems, LIBs employ porous electrodes composed of powdered active material, conductive additives, and polymeric binders. This porous architecture possess interconnected pore networks that facilitate electrolyte infiltration and provide a large electrochemically active interfacial area, thereby enabling good rate capability. However, due to the combined effects of ohmic polarization and concentration polarization, porous electrodes exhibit significant polarization and reaction non-uniformity along the electrode thickness during operation (Figure 2d). Particularly under high-rate fast-charging conditions, these two polarization effects become strongly coupled, resulting in highly uneven potential and current distributions across the graphite anode thickness. Specifically, regions closer to the electrode surface in contact with the separator experience the highest degree of polarization, correspondingly larger local reaction currents, and greater active material utilization, but also a markedly increased propensity for lithium plating.

In porous electrodes, ohmic polarization originates from two conduction pathways: solid-phase and liquid-phase. Structurally, a porous electrode can be viewed as an interpenetrating composite of an electronically conductive phase (active material and conductive additives) and an ionically conductive phase (electrolyte within the pores), as illustrated in Figure 2e. Electrochemical reactions occur at the solid-liquid interface between the two phases, where ionic current is converted into electronic current. In the electrode region near the separator, ionic current (liquid-phase current, I_l) dominates; moving toward the current collector, the current gradually transitions to electronic current (solid-phase current, I_s), which becomes fully dominant at the current collector interface. Accordingly, ohmic polarization exhibits a spatially nonuniform distribution. The electrode surface near the separator is dominated by liquid-phase ohmic polarization (η_l), whereas regions near the current collector are governed primarily by solid-phase ohmic polarization (η_s). The total ohmic polarization (η_Ω) at any position is the sum of these two contributions. For a graphite anode with good electronic conductivity, η_l typically far exceeds η_s, resulting in a pronounced gradient of η_Ω across the electrode thickness: the total ohmic polarization is highest at the electrode surface, where the local current density is also highest and the potential is most negative, making this region highly susceptible to lithium plating during fast charging. To suppress lithium plating, the key is to reduce liquid-phase ohmic polarization. This can be achieved through two principal approaches: (i) employing electrolytes with low bulk resistivity (ρ_l^0), and (ii) engineering electrode architectures with high porosity, reduced thickness (L), and low tortuosity (β), thereby shortening ionic transport pathways and increasing the effective electrolyte volume fraction (V_l). In summary, the overall strategy to reduce ohmic polarization is to combine a high-conductivity electrolyte with a thin, highly porous, low-tortuosity electrode.

Concentration polarization originates from limitations in liquid-phase mass transport of Li^+ ions within the pores of a porous electrode. At high charging rates, the interfacial reaction rate significantly exceeds the diffusion rate of Li^+ in the electrolyte, leading to rapid depletion of Li^+ near the electrode surface and delayed replenishment in the deeper regions, thereby forming a pronounced concentration gradient of Li^+ across the electrode thickness (Figure 2f). The extent of this gradients is governed by several factors, including the chemical diffusion coefficient of Li^+ in the electrolyte (D_0), the Li^+ transference number (t^+), and the electrode porosity and thickness. A higher diffusion coefficient facilitates rapid Li^+ redistribution from high concentration to depleted zones, thereby alleviating concentration gradient and mitigating concentration polarization. Furthermore, the internal electric field during charging makes electromigration non-negligible. A higher t^+ enables the electric field to more effectively drive Li^+ transport toward the anode during charging, enhancing mass transfer and thus helping to lower concentration polarization and improve reaction uniformity across the electrode thickness. Electrode microstructure plays an equally critical role: higher porosity, lower tortuosity,

and smaller thickness all enhance liquid-phase mass transport, thereby suppressing concentration polarization and promoting uniform electrode reaction.

Collectively, the key bottleneck for fast charging LIBs is lithium plating on the graphite anode surface. Effective suppression of lithium plating necessitates synergistic optimization from multiple aspects, including graphite surface chemistry, electrolyte transport properties, and electrode architecture (Figure 3, Table 1). Specifically, for the graphite anode, strategies such as porous structure engineering, edge plane exposure and interlayer transport channel expansion can increase the density of active insertion sites. This, in turn, promotes homogeneous Li^+ intercalation and alleviates interfacial polarization. From the electrolyte perspective, enhancing the Li^+ diffusion coefficient and Li^+ transference number is essential; promising strategies include the use of bulky-anion lithium salts, localized high-concentration electrolytes, and weakly solvating electrolyte systems. At the electrode level, reducing pore tortuosity, decreasing electrode thickness, and increasing porosity are necessary to improve ionic transport within the electrode and reduce ohmic polarization during charging. It should be noted, however, that excessive porosity lowers electrode compaction density and volumetric energy density, while overly thin electrodes similarly compromise energy density. Therefore, optimization graphite anodes for fast-charging is intrinsically a multi-objective synergistic design problem involving graphite active sites, electrolyte properties, and electrode architecture, requiring a systematic balance among fast-charging capability, energy density, and long-term stability.

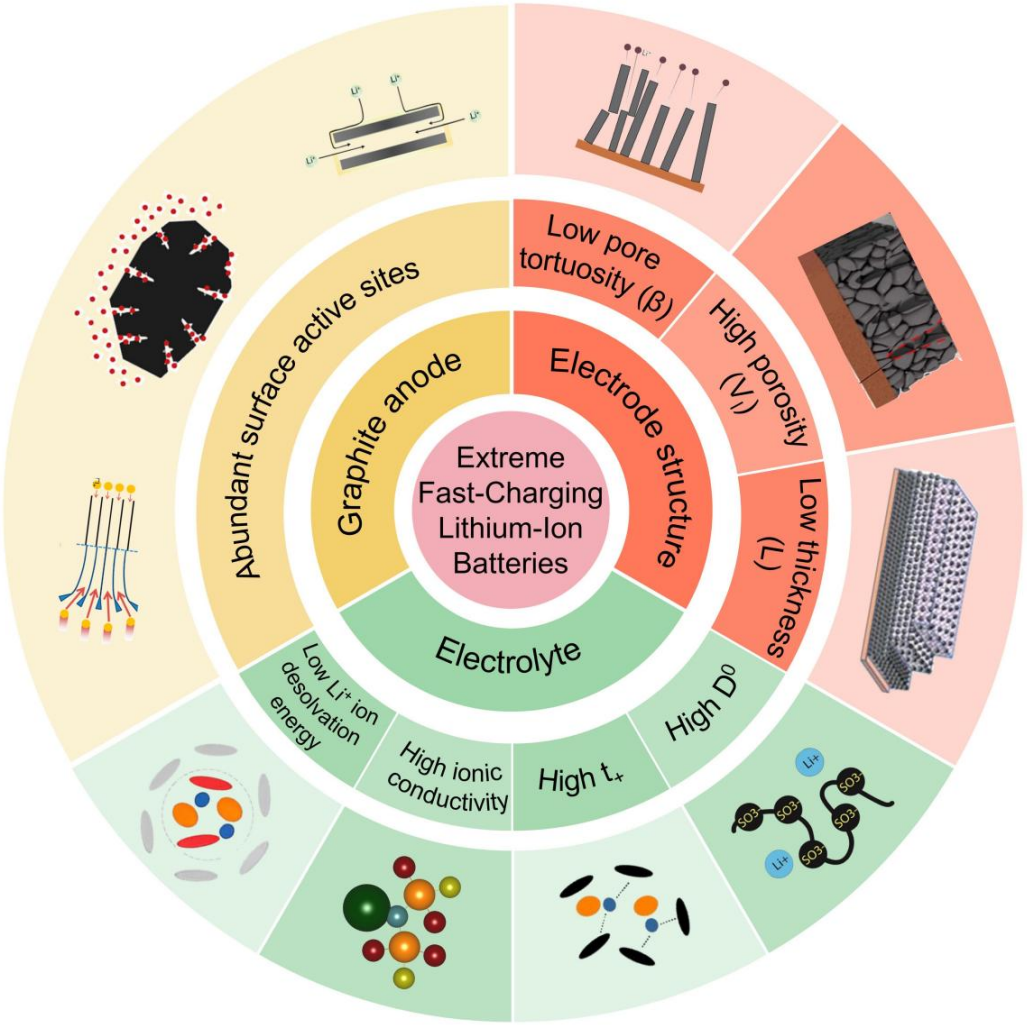

Figure 3. Key factors limiting the fast-charging performance of LIBs and corresponding mitigation strategies.

Table 1. Key factors governing fast-charging performance of LIBs: desired properties, benefits, and practical trade-offs.

Influencing Factors		Fast Charging Requirements	Practicality
Graphite anode	Surface active sites	Abundant	Promotes uniform Li^+ intercalation and mitigates polarization, reducing the risk of lithium plating.
Electrolyte	Li^+ diffusion coefficient (D^0)	High	Enhances Li^+ transport and reduces concentration polarization
	Li^+ transference number (t^+)	High	Enhances Li^+ transport under electric field and promotes uniform reaction across the electrode thickness
	Ionic conductivity	High	Reduces ohmic polarization in the liquid phase
	Li^+ ion desolvation energy	Low	Reduces interfacial polarization and improves reaction kinetics at the graphite surface
Electrode structure	Pore tortuosity (β)	Low	Improves ion transport and lowers tortuosity-induced polarization
	Porosity (V_l)	High	Enhances electrolyte infiltration and reduces ion transport resistance, but lowers compaction density and energy density
	Thickness (L)	Low	Shortens the ion diffusion path and reduces polarization, but lowers energy density

3. Fast Charging Graphite Electrode

As noted above, conventional graphite anodes allow Li^+ intercalation only through the limited edge planes, resulting in a severe shortage of active sites. Therefore, enhancing the fast-charging capability of graphite anodes requires increasing the density of effective Li-intercalation sites on the surface. This can be achieved via strategies such as alkaline etching to generate pores and expose edge planes, expanding the edge structures of graphite layers, and constructing heterogeneous interfaces.

3.1. Etching-Induced Pore Formation to Expose Edge Planes

Strong alkaline etching of graphite generates abundant pore structures (micro-, meso-, and even macropores) on both the surface and in the bulk. This process significantly increases the specific surface area and exposes more active sites for Li^+ intercalation. For example, Cheng et al. [47] stirred natural graphite in 7 M KOH aqueous solution for 12 h, followed by thermal treatment at 800 °C for 1 h under N_2 flow, producing a porous, multichannel architecture (Figure 4a–c). This modification not only increased the number of Li^+ insertion sites but also shortened Li^+ diffusion pathways within the graphite interlayers. Electrochemical measurements showed that the KOH-etched graphite electrode delivered higher capacities than pristine graphite across various charge–discharge rates, demonstrating markedly improved rate capability. In another approach, Kim et al. [48] created porous structures on the graphite surface via a catalytic hydrogenation reaction. Nickel nanoparticles served as catalysts, in which activated hydrogen atoms attacked carbon atoms in the graphite lattice, especially at edges, defect sites, or regions in contact with Ni, etching them into methane (CH_4) that subsequently evolved and left behind micropores. Subsequently, a graphitic carbon shell and an amorphous silicon (a-Si) nanolayer were uniformly deposited on the graphite surface via chemical vapor deposition (CVD) (Figure 4d,e), further increasing the density of surface active sites. As a result, the resulting composite electrode exhibits a 1.5-fold increase in charging rate compared with pristine graphite.

To mitigate structural damage and the decline of initial Coulombic efficiency (ICE) that may result from high-temperature KOH etching, Hu et al. [49] proposed a low-temperature KOH solution etching strategy (Figure 4f). In this approach, graphite was treated in a 20 wt% KOH solution at 95 °C for 12 h under relatively mild conditions. After treatment, uniformly distributed pore structures formed on the graphite surface, which facilitated rapid Li^+ intercalation/deintercalation while significantly improving the fast-charging capability and cycling stability of the graphite anode (Figure 4g,h).

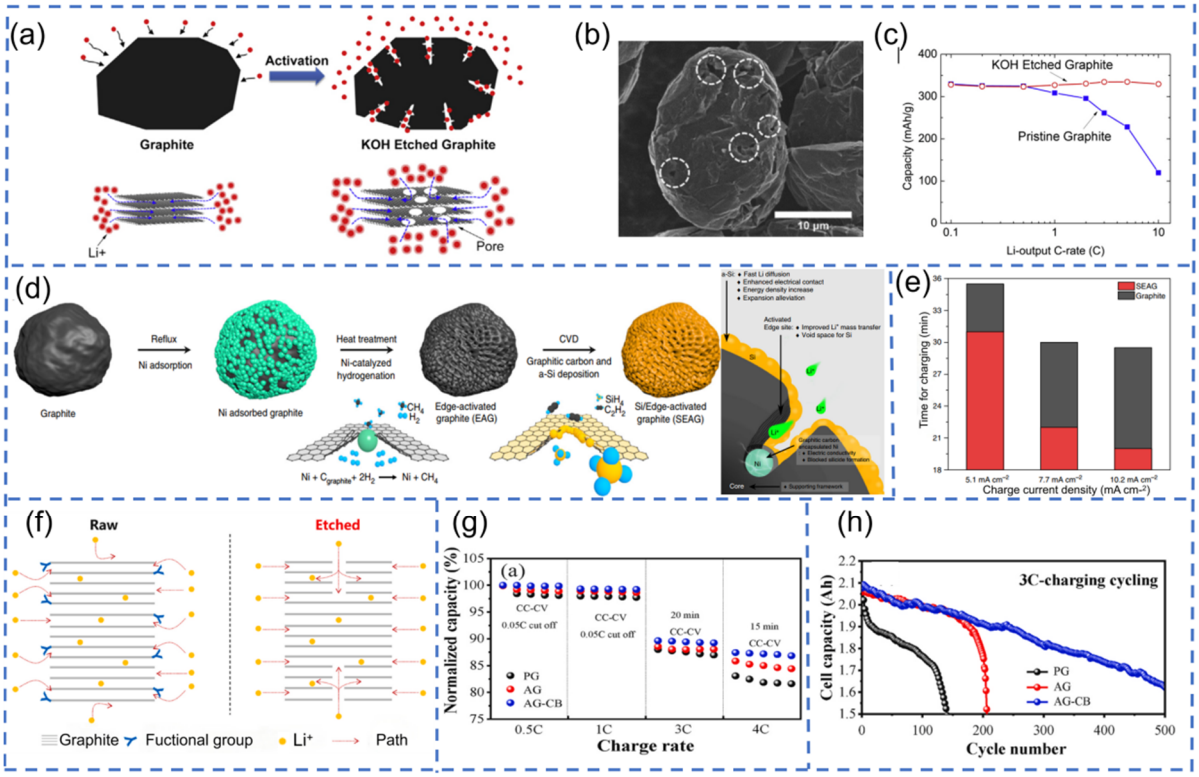

Figure 4. Enhancement of fast-charging performance of graphite via etching-induced pore formation and edge-plane exposure: (**a**–**c**) Strong-alkali etching creates pores and increases active sites. Reproduced with permission [47]. Copyright 2015, Elsevier; (**d**,**e**) Catalytic hydrogenation exposes graphite edge planes. Reproduced with permission [48]. Copyright 2017, Springer Nature; (**f**–**h**) Low-temperature alkaline etching generates uniformly distributed pore channels. Reproduced with permission [49]. Copyright 2024, Elsevier.

3.2. Expanding the Edge Interlayer Spacing of Graphite

Increasing the interlayer spacing at graphite edges (d-spacing > 0.335 nm) can enrich surface active sites, reduce the kinetic barrier for Li^+ diffusion, and alleviate structural distortion of the graphite lattice during Li^+ intercalation. These effects collectively enhance the fast-charging capability of graphite anodes. For instance, Park et al. [50] used direct Friedel-Crafts acylation reactions to selectively functionalize the edges of natural graphite (NG) with different groups, such as fluorobenzoyl and hyperbranched poly(ether ketone), producing FBzCO-NG and HPEK-NG, respectively (Figure 5a). X-ray diffraction (XRD) and X-ray photoelectron spectroscopy (XPS) analyses revealed that functionalization induced structural changes, including increased interlayer spacing (d_0) and reduced crystallite size. At low rates, the functionalized graphite exhibited electrochemical performance comparable to that of pristine graphite. Under high-rate conditions, however, samples with larger d_0 values delivered significantly higher specific capacities. At a 50 C discharge rate, the capacity increased from 110 mA h g^{-1} to 190 mA h g^{-1}, representing nearly a twofold improvement.

Du et al. [51] first subjected graphite to acid treatment, followed by reaction with potassium hydroxide under a reducing atmosphere. During this process, the generated gases (CO_2 and H_2O) penetrated the graphite bulk, promoting interlayer expansion. Meanwhile, the vigorous volatilization of unevenly distributed potassium at high temperatures exerted additional stress on the graphite edges, inducing edge bending and activation, which ultimately produced graphite with gas-activated edges (GWAE). These activated edges not only increase the number of Li^+ intercalation sites (Figure 5b) but also endowed the material with excellent fast-charging performance in both half-cells and full cells. Specifically, GWAE delivered a reversible capacity of 150.3 mA h g^{-1} at 10 C, and maintained a capacity retention of 96.05% after 700 cycles at 5 C.

Similarly, Yao et al. [30] proposed using the ratio of aromatic bridging carbon to peripheral aromatic carbon in the precursor (defined as XBP) as a key structural descriptor, and systematically investigated its influence on interlayer spacing and high-rate Li storage performance. A higher XBP corresponds to a greater proportion of aromatic bridging carbon, which results in a higher degree of graphitization and a slightly expanded interlayer spacing (0.3373–0.3384 nm vs. 0.3354 nm for natural graphite). This is because a higher XBP suppresses low-temperature cross-linking reactions and promotes the formation of ordered, slightly expanded layered structures.

As XBP increased from 0.212 (BCG125) to 0.486 (BCG135), the discharge capacity at 5 C increased from 92 mA h g^{-1} to 201 mA h g^{-1}, exhibiting a pronounced parabolic growth relationship.

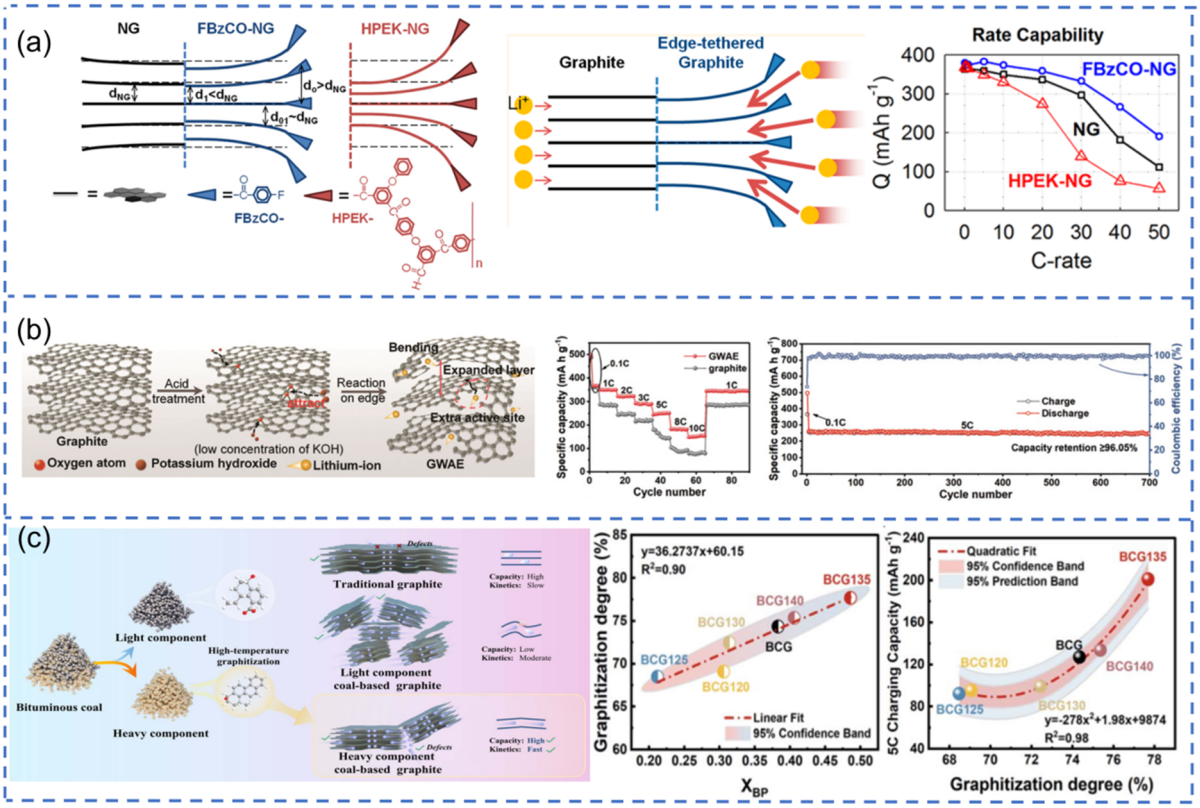

Figure 5. Enhancement of fast-charging performance of graphite via interlayer expansion: (**a**) Edge functionalization-induced layer expansion. Reproduced with permission [50]. Copyright 2012, American Chemical Society; (**b**) Gas-activated edge expansion. Reproduced with permission [51]. Copyright 2022, Royal Society of Chemistry; (**c**) Regulation of graphite interlayer spacing via precursor aromatic structure engineering. Reproduced with permission [30]. Copyright 2025, Royal Society of Chemistry.

3.3. Constructing Heterogeneous Interfaces

Constructing heterostructures on the electrode surface is another effective strategy to enrich the active sites of graphite anodes. For example, Cai et al. [52] coated graphite with a nanoscale amorphous carbon layer (Figure 6a). This carbon coating not only provided abundant active sites but also created additional Li^+ diffusion pathways on the graphite basal planes, thereby significantly alleviating reaction polarization. Even without noticeable changes in Li^+ desolvation energy and SEI penetration barrier, the introduction of this heterostructure substantially increased the exchange current density, confirming that increased surface active sites are key to enabling fast charging (Figure 6b–d). Similarly, Du et al. [53] anchored lithiophilic hard carbon onto the graphite surface. Owing to the isotropic structure and abundant active sites of hard carbon, this design enhanced the lithiophilicity of the graphite surface while providing additional Li^+ insertion sites. The resulting graphite electrode exhibited outstanding fast-charging durability, retaining 90.1% of its capacity after 4000 cycles at a high rate of 10 C (Figure 6e,f).

In addition, constructing metal-graphite heterostructures can also enhance the fast-charging performance of graphite anodes. Sheng et al. [33] designed a $Nb_2O_5/Zr_6Nb_2O_{17}$-graphite heterostructured composite, which increases surface active sites while generating a built-in electric field (BIEF) at the heterojunction interface. This internal field drives directional Li^+ transport along the electric field gradient, thereby reducing concentration polarization and enabling fast charging of the graphite electrode at 6 C (Figure 6g,h).

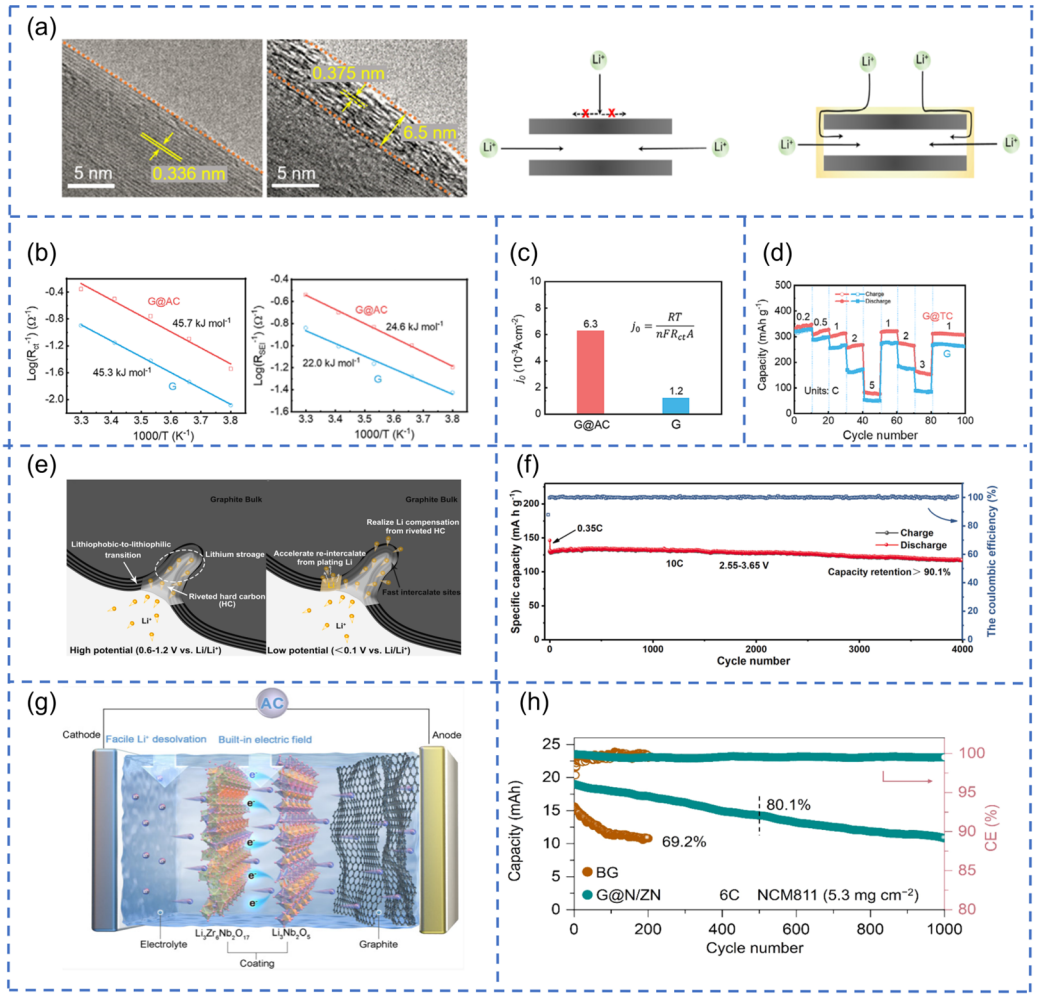

Figure 6. Construction of heterostructures to enhance the fast-charging performance of graphite anodes: (**a**–**d**) Amorphous carbon coating on graphite. Reproduced with permission [52]. Copyright 2020, John Wiley and Sons; (**e**,**f**) Lithiophilic hard carbon anchored onto graphite. Reproduced with permission [53]. Copyright 2025, American Chemical Society; (**g**,**h**) Metal oxide heterostructure-modified graphite. Reproduced with permission [33]. Copyright 2025, American Chemical Society.

3.4. Accelerating Li^+ Desolvation

As discussed in the introduction, the Li^+ desolvation process represents a key kinetic bottleneck limiting the fast-charging capability of anodes. Therefore, reducing the Li^+ desolvation energy is an effective strategy to improve fast-charging performance. As the innermost interfacial layer between the graphite anode and the electrolyte, the SEI plays a critical role in regulating the Li^+ desolvation process. The chemical composition, thickness, and structural homogeneity of the SEI directly influence the local solvation environment of Li^+ at the electrode/electrolyte interface. A widely adopted approach involves constructing an artificial SEI on the anode surface, which weakens the interaction between Li^+ and solvent molecules and thereby lowers the Li^+ desolvation energy barrier. For example, Li et al. [54] reduced the solvation energy by uniformly coating graphite particles with a copolymer layer composed of polyethylene glycol phenyl ether (PEGPE) and poly(allylamine) (PAAm). This polymer layer adhered tightly to the graphite surface through π-π stacking interactions between aromatic rings and graphite, while the lone electron pairs on ether bonds coordinated with Li^+ ions passing through the coating, effectively promoting the desolvation process. As a result, the modified graphite anode delivered a high discharge capacity of 336 mA h g^{-1} at 10 C (Figure 7a,b). Similarly, Song et al. [55] introduced a poly(2,4-hexadiene-1,6-diol) coating (LMA) on a lithium metal anode. The hydroxyl groups on the coating surface formed hydrogen bonds with electrolyte solvent molecules, facilitating Li^+ desolvation. Meanwhile, the ordered -OLi structure within the coating guided the rapid and directional migration of Li^+. Full cells assembled with this modified anode (LMA | $LiNi_{0.8}Co_{0.1}Mn_{0.1}O_2$) exhibited excellent capacity retention and long-term cycling stability at high rates (Figure 7c).

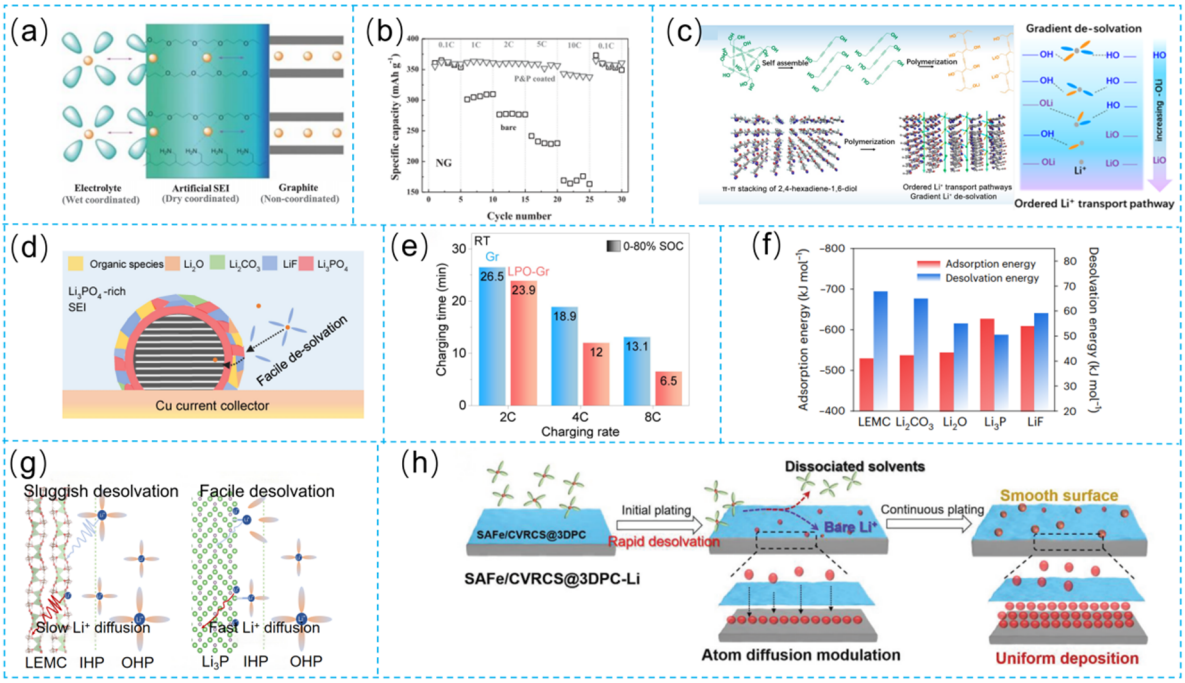

Figure 7. Artificial SEI engineering to accelerate Li^+ desolvation and enhance the fast-charging performance of graphite anodes: (**a**) Schematic of the PEGPE-PAAm copolymer coating mechanism on graphite. Reproduced with permission [54]. Copyright 2014, John Wiley and Sons; (**b**) Rate capability comparison of PEGPE-PAAm-coated graphite anodes. Reproduced with permission [54]. Copyright 2014, John Wiley and Sons; (**c**) Hydrogen-bond interaction between hydroxyl groups in the poly(2,4-hexadiene-1,6-diol) coating and solvent molecules, facilitating Li^+ desolvation. Reproduced with permission [55]. Copyright 2023, American Chemical Society; (**d**) Mechanism of Li^+ desolvation facilitated by the low work function of Li_3PO_4. Reproduced with permission [56]. Copyright 2024, John Wiley and Sons; (**e**) Comparison of charging time to 80% state of charge (SOC) for graphite anodes at different rates before and after Li_3PO_4 modification. Reproduced with permission [56]. Copyright 2024, John Wiley and Sons; (**f**) Influence of different SEI components on the Li^+ desolvation energy of graphite anodes. Reproduced with permission [57]. Copyright 2023, Spring Nature; (**g**) Mechanism of Li_3P-assisted Li^+ desolvation. Reproduced with permission [57]. Copyright 2023, Spring Nature; (**h**) Single-atom catalysts reduce the interfacial desolvation energy. Reproduced with permission [58]. Copyright 2023, John Wiley and Sons.

In addition, inorganic electron-donor interfacial layers can also accelerate Li^+ desolvation. Wang et al. [56] constructed SEI layers enriched with LiF, Li_2CO_3, or Li_3PO_4 on the graphite surface. Compared with Li_2CO_3 (work function 6.0 eV) and LiF (7.6 eV), Li_3PO_4 has a lower work function (5.2 eV) and thus acts as an electron donor. This property weakens the interaction between Li^+ and solvent molecules, thereby facilitating Li^+ desolvation. Full cells assembled with the Li_3PO_4-modified graphite anode (LPO-Gr) were capable of charging to 80% capacity within 6.5 min (Figure 7d–f). Similarly, Tu et al. [57] reported that Li_3P exhibits the strongest affinity for Li^+ among conventional inorganic SEI components such as Li_2O, Li_2CO_3, and LiF. This strong affinity induces a low-solvent-coordination Li^+ solvation structure near the inner Helmholtz plane (IHP) at the electrode/electrolyte interface, significantly reducing the Li^+ desolvation energy. By constructing an ultrathin sulfur-bridged phosphorus layer on the graphite surface, which in situ converts into a crystalline Li_3P-based SEI with high ionic conductivity during cycling, the Li^+ desolvation process was effectively accelerated. Benefiting from this optimized SEI structure, the assembled pouch cell (P-S graphite||$LiNi_{0.6}Co_{0.2}Mn_{0.2}O_2$) delivered a discharge capacity at 10 C corresponding to 80% of its capacity at 0.2 C (Figure 7g).

Furthermore, the interfacial catalysis strategy represents an emerging yet effective approach to reduce the desolvation energy barrier. Passerini et al.[58]. anchored iron single atoms (SAFe) onto cation-vacancy-rich cobalt sulfide ($Co_{1-x}S$) nanoparticles, which were embedded in a three-dimensional porous carbon (3DPC) framework, forming an interfacial catalytic layer (SAFe/CVRCS@3DPC). In conventional electrolytes, the stepwise dissociation of Li^+ solvation structures (e.g., $Li(DME)_4^+$) requires overcoming an energy barrier as high as 36.84 kJ mol^{-1}. Upon introducing the catalyst, when $Li(DME)_4^+$ or $Li(DOL)_4^+$ complexes come into contact with the SAFe/CVRCS catalyst surface, the Gibbs free energy change (ΔG) of the desolvation process becomes negative ($\Delta G < 0$), indicating that the

reaction becomes thermodynamically spontaneous and proceeds without additional energy consumption. Through this approach, low polarization and high specific capacity were achieved at a 5 C rate. (Figure 7h).

4. Fast-Charging Electrolytes

Electrolytes influence the fast-charging performance of anodes primarily by regulating charge transport and interfacial reactions, manifesting in three key aspects: (1) Electrolyte-phase resistance causes pronounced ohmic polarization and non-uniform potential distribution along the electrode thickness. Increasing the ionic conductivity of the electrolyte can effectively mitigate such polarization. (2) During fast charge-discharge, Li^+ concentration gradients readily develop within the electrode, leading to concentration polarization. Increasing the Li^+ diffusion coefficient and transference number helps alleviate these gradients. (3) The Li^+ desolvation step at the anode surface is often the rate-determining step of the interfacial reaction. Lowering the desolvation energy barrier significantly accelerates interfacial reaction kinetics and reduce electrochemical polarization. Therefore, we will systematically discuss the design and optimization of fast-charging electrolytes from four perspectives: increasing ionic conductivity, enhancing the Li^+ diffusion coefficient, improving the Li^+ transference number, and reducing the Li^+ desolvation energy.

4.1. Increasing Ionic Conductivity

A comparison of commonly used electrolyte solvents (Figure 8a) [16] shows that no single solvent simultaneously offers both a high dielectric constant and low viscosity, as each has trade-offs in terms of electrochemical stability window, viscosity (η), and dielectric constant (ε). Consequently, multicomponent solvent formulations have become a widely adopted strategy to enhance ionic conductivity.

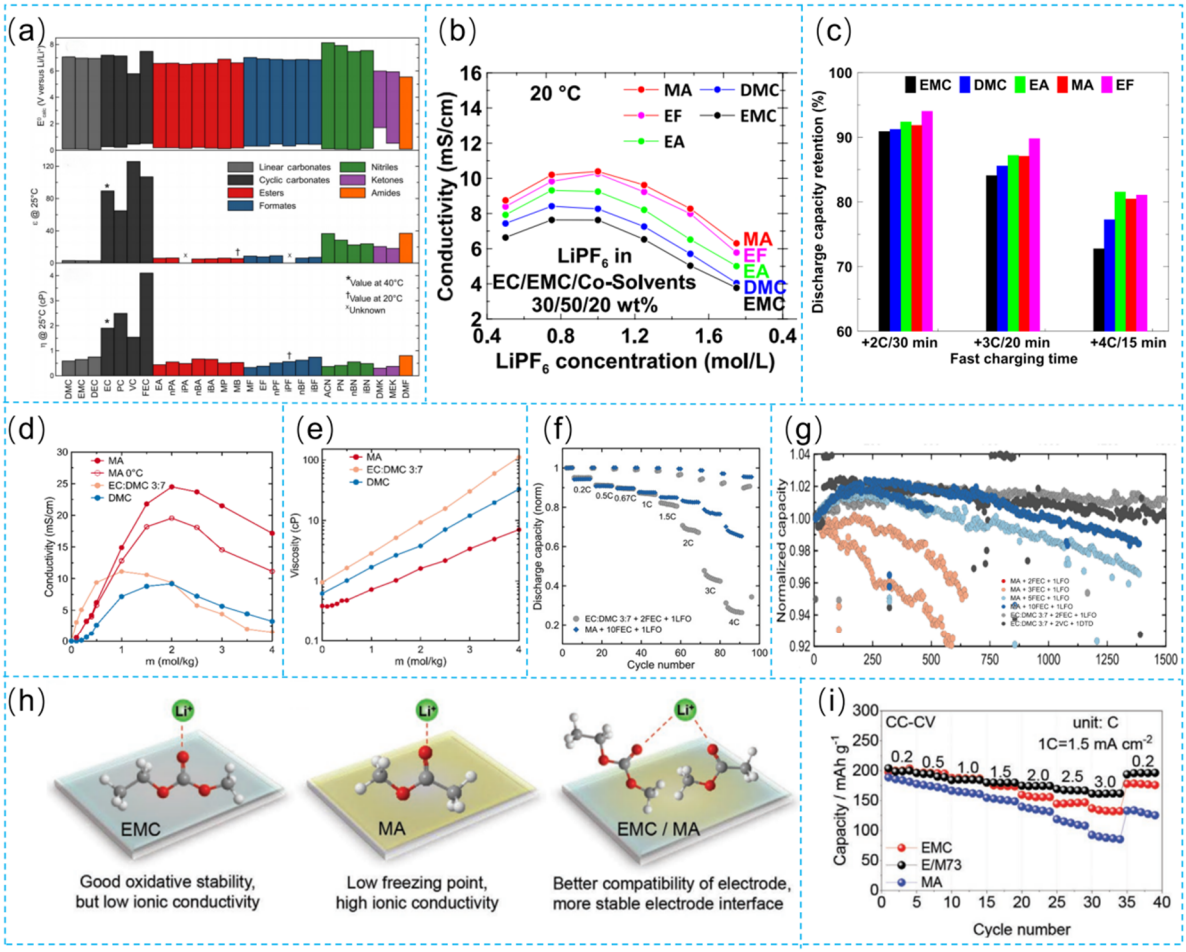

Figure 8. Electrolyte optimization using low-viscosity co-solvents and its impact on fast-charging performance: (**a**) Comparison of the physicochemical properties of commonly used electrolyte solvents. Reproduced with permission [16]. Copyright 2020, Elsevier; (**b**) Effect of different co-solvents on the ionic conductivity of EC/EMC-based electrolytes. Reproduced with permission [59]. Copyright 2020, Institute of Physics; (**c**) Rate capability of cells with low-viscosity co-solvents (DME/EA/MA/EF). Reproduced with permission [59]. Copyright 2020,

Institute of Physics; (**d**,**e**) Influence of MA co-solvent on electrolyte conductivity and viscosity Reproduced with permission [60]. Copyright 2020, Elsevier; (**f**,**g**) Effects of FEC and LFO additives on the rate capability and cycling stability of cells using low-viscosity co-solvent electrolytes. Reproduced with permission [61]. Copyright 2020, Amercian Chemical Society; (**h**) Advantages of EC-free electrolytes. Reproduced with permission [62]. Copyright 2021, John Wiley and Sons; (**i**) Rate capability of cells employing an EC-free electrolyte (1.2 M $LiPF_6$ in EMC:MA = 7:3). Reproduced with permission [62]. Copyright 2021, John Wiley and Sons.

4.1.1. Introduction of Low-Viscosity Co-Solvents

One effective strategy to enhance ionic conductivity is the introduction of a low-viscosity co-solvent into the base electrolyte. For instance, 1,2-dimethoxyethane (DME) and ethyl acetate (EA) exhibit significantly lower viscosities than conventional carbonate solvents such as ethyl methyl carbonate (EMC) and ethylene carbonate (EC), while DME also possesses a higher dielectric constant than EA. When a co-solvent is introduced into the EC/EMC electrolyte system, the ionic conductivity of electrolyte follows the order: EC/EMC-DME > EC/EMC-EA > EC/EMC, and the corresponding rate performance of the batteries improves accordingly [59]. In a similar study, Wu et al. [60] further quantified the conductivity enhancement of the EC/EMC system using different co-solvents, ranking them as methyl acetate (MA) > ethyl formate (EF) > EA > dimethyl carbonate (DMC). Electrolytes containing these co-solvents all exhibited superior fast-charging performance (Figure 8b–e).

However, the introduction of low-viscosity co-solvents may compromise the stability of SEI, thereby adversely affecting the cycling life of the battery. To mitigate this issue, Dahn et al. [61] combined film-forming additives, including fluoroethylene carbonate (FEC) and lithium difluorophosphate ($LiPO_2F_2$, LFO), with low-viscosity co-solvents. This strategy simultaneously reduced electrolyte viscosity and stabilized the SEI. As a result, the battery achieved a discharge capacity at 4 C that was 65% of its capacity at 0.2 C, along with significantly improved cycling stability (Figure 8f,g). Furthermore, although EC facilitates the formation of a stable SEI, its relatively high viscosity limits the ionic conductivity of the electrolyte (Figure 8h). To overcome this limitation, Ming et al. [62] developed an EC-free electrolyte formulation: 1.2 M $LiPF_6$ in EMC:MA (7:3 *v*/*v*). This system maintains a high initial Coulombic efficiency (>90%) while significantly increasing ionic conductivity and reducing interfacial resistance, ultimately enabling excellent high-rate performance (Figure 8i).

4.1.2. Designing High-Conductivity Lithium Salts

Selecting or designing lithium salts that readily dissociate and impart low viscosity to the electrolyte is an effective strategy for enhancing electrolyte conductivity. In conventional carbonate-based electrolytes, the room-temperature ionic conductivity of commonly used lithium salts generally follows the order: LiFSI > $LiPF_6$ > LiTFSI > $LiClO_4$ > $LiBF_4$ (Figure 9a). Among these salts, LiFSI exhibits superior performance owing to its larger anion radius, higher degree of dissociation, and more favorable solvation environment with solvent molecules. At room temperature, the ionic conductivity and Li^+ transference number (t^+) of LiFSI-based electrolytes can reach 10.36 mS cm^{-1} and 0.495, respectively, both higher than those of the widely used $LiPF_6$ electrolyte (9.35 mS cm^{-1} and 0.382). Studies have shown that replacing $LiPF_6$ with LiFSI in the same solvent system (e.g., EC/EMC) significantly improves battery performance at high rates. Under 5 C fast-charging conditions, the battery exhibited higher discharge capacity and reduced lithium dendrite deposition (Figure 9b,c) [63].

However, LiFSI corrodes aluminum current collectors at high potentials (>3.7 V vs. Li^+/Li), limiting its direct application in high-voltage cathode systems. To address this issue, a multi-salt synergistic strategy has been proposed. Zheng et al. [64] developed a ternary lithium-salt electrolyte composed of LiFSI, LiBOB (lithium bis(oxalato)borate), and $LiPF_6$. In this system, LiFSI primarily provides high ionic conductivity, while LiBOB forms a dense and stable passivation layer in situ on the Al current collector, effectively suppressing corrosion. Meanwhile, $LiPF_6$ maintains interfacial stability across a wide voltage window. This synergistic electrolyte design preserves excellent ion transport properties while significantly improving compatibility with high-voltage cathodes, thereby enabling comprehensive optimization of battery performance at high rates (Figure 9d).

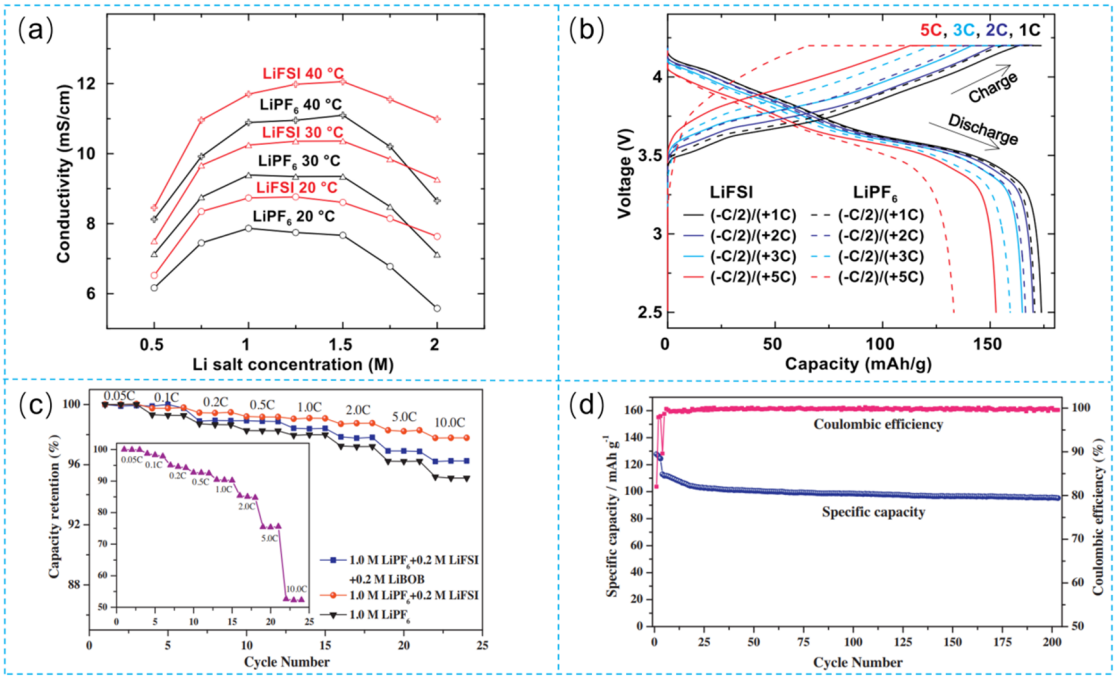

Figure 9. Influence of high-conductivity lithium salts on fast-charging performance: (**a**) Effect of different lithium salts on electrolyte conductivity. Reproduced with permission [63]. Copyright 2019, Elsevier; (**b**) Rate performance of cells with LiFSI replacing $LiPF_6$ as the lithium salt. Reproduced with permission [63]. Copyright 2019, Elsevier; (**c**,**d**) Electrochemical performance of cells using a LiFSI/LiBOB/$LiPF_6$ ternary-salt electrolyte system. Reproduced with permission [64]. Copyright 2014, Elsevier.

4.2. Increasing the Li^+ Diffusion Coefficient

The diffusion coefficient of Li^+ in the electrolyte is a key parameter governing mass transport kinetics during fast charging. As summarized in Table 2, the Li^+ diffusion coefficient in conventional LIB electrolytes typically lies in the range of 10^{-6} to 10^{-5} cm^2 s^{-1} [16]. Notably, even when the lithium-salt concentration is increased to 4 mol L^{-1}, the Li^+ diffusion coefficient remains within the same order of magnitude. This phenomenon is primarily attributed to the solvation effect, which effectively averages the ionic radii of the solvated species in the electrolyte. In typical LIB electrolytes, the diffusion coefficients follow the relationship: $D_{Li+} < D_{anion} < D_{solvent}$ [65–67].

According to the Stokes-Einstein relation, the diffusion coefficient of Li^+ (D) can be expressed as:

$$D = kT/(6\pi\eta r_s)$$

where k is the Boltzmann constant, T is the absolute temperature, r_s is the solvation radius of Li^+, and η is the electrolyte viscosity.

From this equation, it is evident that reducing the solvation radius (r_s) and electrolyte viscosity (η) can effectively increase the D_{Li+}.

One practical approach to achieving this is to use solvents with weaker coordination ability, which leads to a looser Li^+ solvation sheath, thereby reducing the effective solvation radius and lowering the overall viscosity. For example, in a 2 M $LiPF_6$/MA-FEC electrolyte system (Figure 10a–c), MA exhibited significantly weaker coordination with Li^+ compared to EC and DMC. The average coordination numbers follow the order: EC ≈ 5 > DMC ≈ 3.5 > MA ≈ 2.5. This weak coordination results in a more loosely structured solvation shell, reducing the effective solvation radius (r_s) while simultaneously decreasing the system viscosity (η). Consequently, the mass transport of Li^+ is significantly enhanced, leading to improved fast-charging capability and low-temperature performance of the battery [61].

Another effective strategy is the construction of localized high-concentration electrolytes (LHCEs) [68]. In this approach, a low-viscosity, non-coordinating (or weakly coordinating) inert diluent such as a fluorinated ether, is introduced into a conventional high-concentration electrolyte. Since the diluent does not participate in the primary Li^+ solvation sheath, the electrolyte retains the characteristic solvation structure of high-concentration systems while its overall viscosity is substantially reduced (Figure 10d,e). This unique combination of a high-concentration structure with low-viscosity behavior effectively increases the Li^+ diffusion coefficient, thereby improving the high-rate performance of LIBs.

Table 2. Self-diffusion coefficients of pure solvents and of solvent molecules, Li^+, and $TFSI^-$ anions in 1 M LiTFSI solutions, along with ionic conductivities and degrees of dissociation, measured at 30 °C in various solvents.

	Diffusion Coefficient (10^{-10} m^2s^{-1})				Ionic Conductivity (10^{-3} S cm)	Degree of Dissociation
	Pure Solvent (^{1}H NMR)	Solvent (^{1}H NMR)	$N(SO_2CF_3)_2$ (^{19}H NMR)	Lithium (^{7}Li NMR)		
EC[a]	8.0	4.3	3.1	2.1	8.3	
PC	5.8	3.5	2.6	1.6	5.2	0.62
BC	4.5	2.6	2.0	1.2	3.5	0.64
GBL	9.0	5.3	3.8	2.5	8.9	0.64
GVL	8.1	5.0	3.4	2.1	6.4	0.65
NMP	8.2	5.1	3.7	2.4	2.0	0.18
TG	6.1	4.6	3.0	2.6	2.0	0.37
DG	13	9.3	5.0	4.5	4.5	0.38
DEE	22	15	6.1	6.1	1.8	0.12
DME	31.5	22	8.8	7.7	8.9	0.31
DOx	25.5	17	6.2	6.4	3.1	0.10
THF	30	13	7.3	5.9	10.6	0.36
EP	25	17	7.3	7.5	6.7	0.27
DMC	26	16	6.0	5.8	2.7	0.11

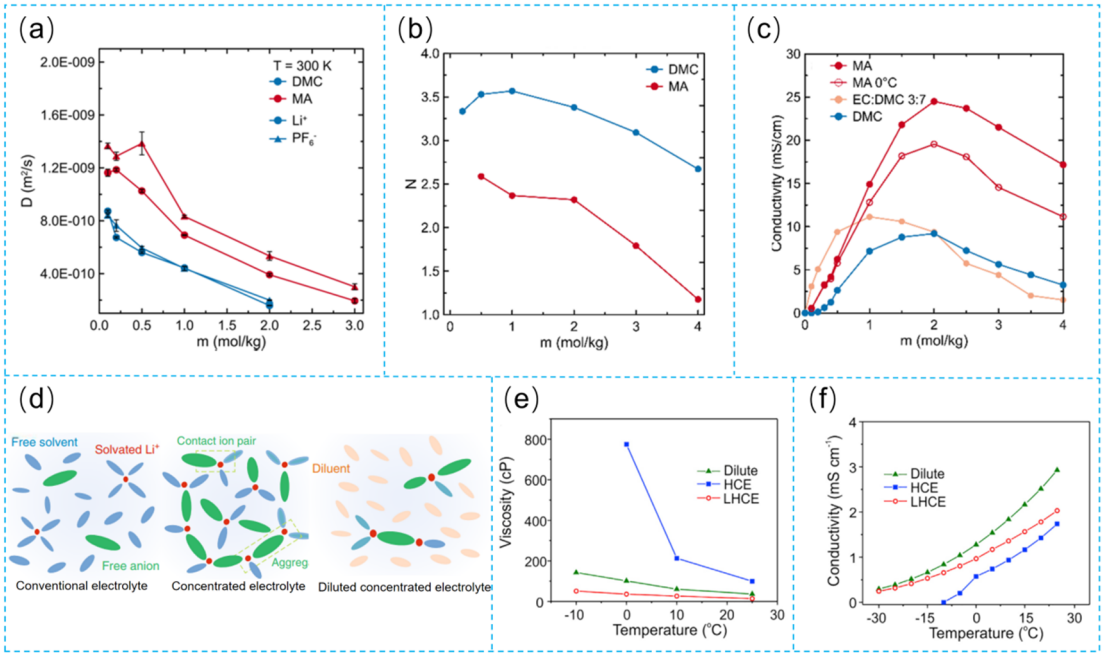

Figure 10. Enhancement of the Li^+ diffusion coefficient using weakly coordinating solvents: Comparison of the diffusion coefficient (**a**), solvation number (**b**), and ionic conductivity (**c**) when MA and DMC are used as electrolyte solvents. Reproduced with permission [58]. Copyright 2012, American Chemical Society; Comparison of anion pairing behavior (**d**), viscosity (**e**), and ionic conductivity (**f**) among conventional electrolytes, high-concentration electrolytes (HCE), and localized high-concentration electrolytes (LHCE). Reproduced with permission [68]. Copyright 2018, Elsevier.

4.3. Increasing the Li^+ Transference Number

The ionic conductivity (σ) of an electrolyte reflects its instantaneous charge-transport capability and is jointly contributed by both cations and anions. The Li^+ transference number (t^+) represents the fraction of total current carried specifically by Li^+ ions and is defined as:

$$t_+ + t_- = 1$$

where t_+ and t_- denote the transference numbers of the cation (Li^+ in LIBs) and the anion, respectively.

In LIBs, Li^+ is the only charge carrier participating in electrode reactions. Therefore, a higher t_+ corresponds to more efficient Li^+ mass transport, which helps suppress concentration polarization and thereby improves rate capability. As shown in Figure 11a, graphite/$LiCoO_2$ cells using electrolytes with different t_+ values exhibited markedly different internal Li^+ concentration distributions. A higher t_+ leads to a smaller Li^+ concentration gradient within the electrode and a weaker concentration polarization [69]. When the ionic conductivity of the electrolyte is

kept constant, the rate performance of the battery continuously improves with increasing t_+ (Figure 11b). However, the t_+ of conventional carbonate-based electrolytes is typically only 0.35–0.4 (Figure 11c) [16]. This limitation arises because solvent molecules coordinate with Li^+ to form a solvation sheath, which increases the effective size of the migrating species and consequently reduces its mobility. Thus, the fundamental strategy for increasing t_+ is to restrict anion mobility. Common approaches include the use of lithium salts with bulky anions, the design of anion-immobilized functional structures, and the construction of high-concentration electrolyte systems.

Compared with PF_6^-, the TDI anion (4,5-dicyano-2-(trifluoromethyl)imidazole) possesses a significantly larger ionic size. In an EC:DEC:DMC solvent system, simply replacing $LiPF_6$ with LiTDI increased the Li^+ transference number from 0.24 to 0.50 [70]. Similarly, using LiTTP (lithium tetra(trifluoromethanesulfonyl)phosphate) can further raise t_+ to approximately 0.7 (Figure 11d) [71]. In addition to using bulky anions, direct immobilization of anions is another effective strategy for enhancing t_+ [72]. For example, polyanionic electrolytes can significantly suppress anion diffusion while exerting minimal influence on cation transport, yielding t_+ values as high as 0.98 (Figure 11e,f) [73].

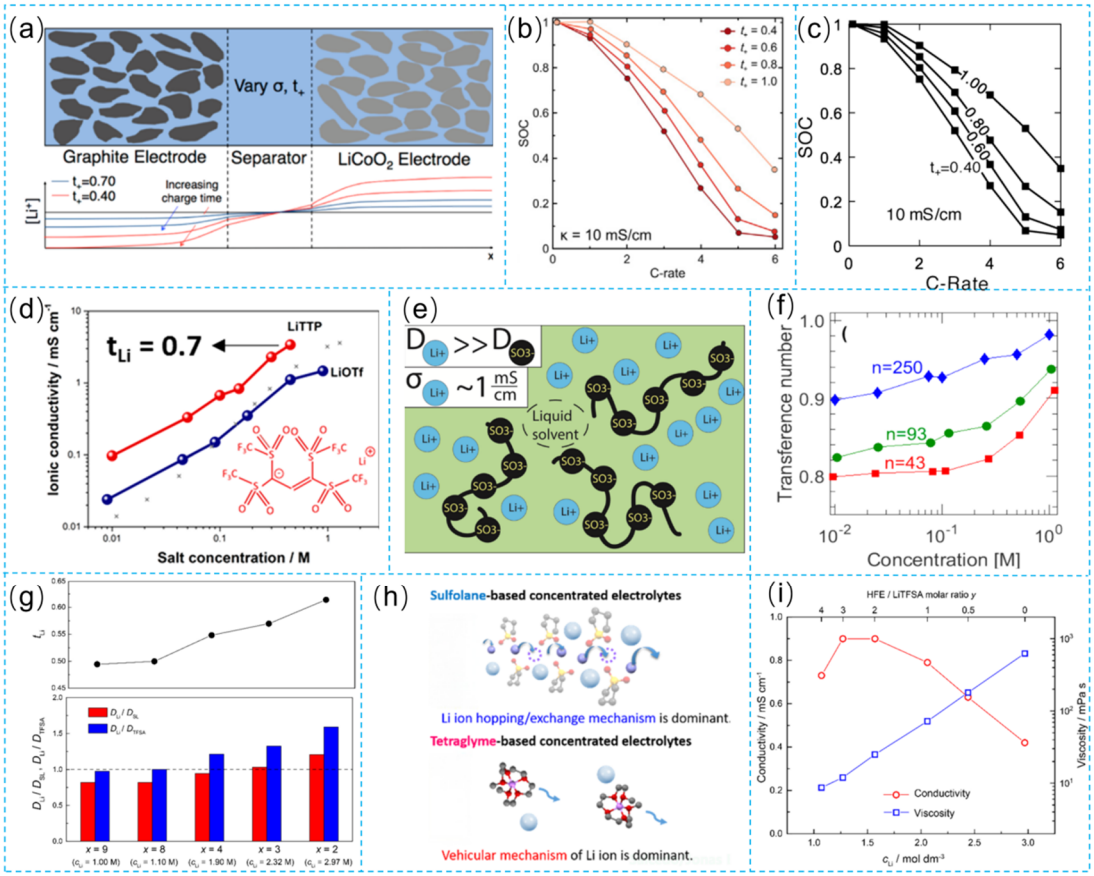

Figure 11. Regulation mechanisms of the Li^+ transference number and their impact on electrochemical performance: (**a**) Internal Li^+ concentration polarization distributions in graphite/$LiCoO_2$ cells using electrolytes with different t_+ values. Reproduced with permission [69]. Copyright 2017, American Chemistry Society; (**b**) Rate capability as a function of increasing t_+ at constant ionic conductivity. Reproduced with permission [16]. Copyright 2020, Elsevier; (**c**) Typical t_+ range of conventional carbonate-based electrolytes. Reproduced with permission [16]. Copyright 2020, Elsevier; (**d**) Enhancement of t_+ using lithium salts with bulky anions. Reproduced with permission [71]. Copyright 2018, American Chemistry Society; (**e**) Improvement of t_+ using polyanionic electrolytes. Reproduced with permission [73]. Copyright 2017, American Chemistry Society; (**f**) Influence of the weight-average molecular weight of polyanionic electrolytes on t_+. Reproduced with permission [73]. Copyright 2017, American Chemistry Society; (**g**) Effect of lithium-salt concentration on t_+ in HCEs. Reproduced with permission [74]. Copyright 2019, American Chemistry Society; (**h**) Li^+-hopping conduction mechanism in HCEs. Reproduced with permission [74]. Copyright 2019, American Chemistry Society; (**i**) Influence of the diluent HFE on the viscosity of HCEs. Reproduced with permission [75]. Copyright 2019, American Chemistry Society.

Another approach involves increasing the lithium-salt concentration (typically to 3–5 mol L^{-1}), which shifts the Li^+ transport mechanism from the conventional vehicle mechanism to a structural diffusion (ion-hopping) mechanism. In HCEs, the abundance of ion pairs and aggregates results in a more compact Li^+ solvation sheath and

facilitates this hopping conduction, thereby increasing t_+ values up to approximately 0.73 (Figure 11g,h) [74,75]. Introducing diluents such as hydrofluoroethers (HFE) to form LHCEs can retain the advantage of high t_+ while simultaneously lowering viscosity (Figure 11i) [75]. Nevertheless, these high-t_+ strategies often come with increased electrolyte viscosity and reduced ionic conductivity. For instance, the aforementioned polyanionic electrolyte with t_+ ≈ 0.98 exhibited an ionic conductivity of only ~1 mS cm^{-1}. Similarly, the conductivity of HCEs typically remains below 3 mS cm^{-1}. Elevated viscosity can hinder electrolyte infiltration into the porous structure of thick electrodes, resulting in poor interfacial contact and a reduced effective reaction area, which ultimately fails to meet the low-impedance requirements for extreme fast charging. Therefore, the design of next-generation electrolytes must achieve a synergistic balance among high Li^+ transference number (t_+), low viscosity (η), and high ionic conductivity (σ).

4.4. Reducing the Desolvation Energy

As discussed previously, the Li^+ desolvation process at the graphite anode represents the rate-determining step during charging (Figure 12a). Lowering the desolvation energy barrier can significantly enhance the interfacial reaction kinetics of graphite anodes, typically manifested as an increase in the exchange current density (i^0). Differences in the molecular structure and coordination ability of solvents provide a fundamental basis for regulating Li^+ desolvation energy. As illustrated in Figure 12b, the desolvation energy of common solvents generally increases in the following order: nitro compounds < ethers < sulfites < nitriles < carbonates < lactones < sulfones < amides < phosphates < dinitriles [16]. Based on this trend, employing solvents with low desolvation energy is one of the most direct and effective strategies. For example, Fan et al. [31] used 1.8 M LiFSI in 1,3-dioxolane (DOL) as a fast-charging electrolyte. Although DOL exhibits relatively low ionic conductivity (Figure 12c), its low desolvation energy (Figure 12d) effectively accelerates the interfacial reaction, enabling ultrafast charging at 50 C (Figure 12e).

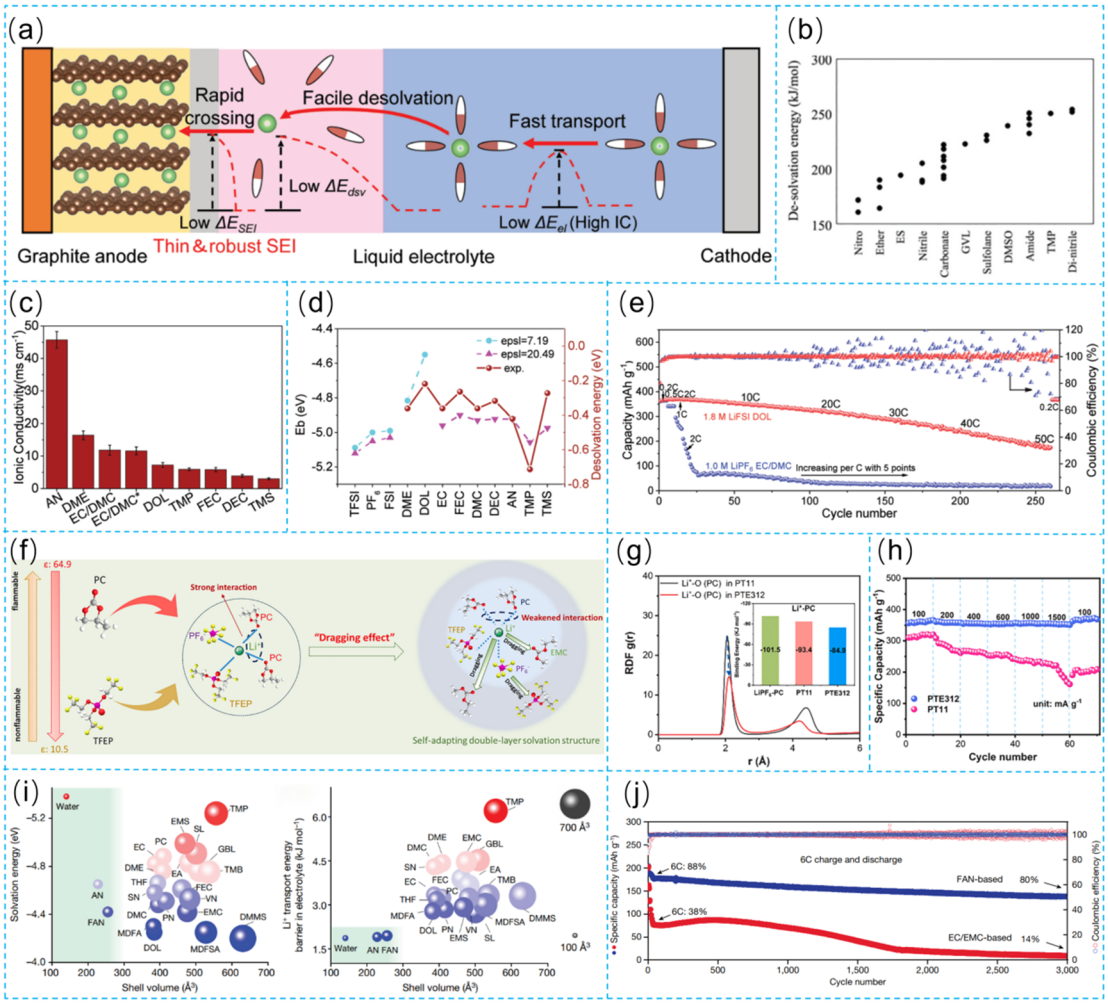

Figure 12. Strategies for regulating Li^+ desolvation energy and their influence on fast-charging performance: (**a**) Distribution of interfacial reaction energy barriers at the graphite anode during charging. Reproduced with permission [31]. Copyright 2022, John Wiley and Sons; (**b**) Comparison of desolvation energies of different

solvents. Reproduced with permission [16]. Copyright 2020, Elsevier; (**c**) Ionic conductivity of various electrolyte solvents. Reproduced with permission [31]. Copyright 2022, John Wiley and Sons; (**d**) Desolvation energies of representative solvents. Reproduced with permission [31]. Copyright 2022, John Wiley and Sons; (**e**) Fast-charging performance of a graphite electrode in 1.8 M LiFSI/DOL electrolyte. Reproduced with permission [31]. Copyright 2022, John Wiley and Sons; (**f**,**g**) Solvation structure, Li^+-solvent coordination configuration, and rate performance of graphite after introducing TFEP into a PC-based electrolyte. Reproduced with permission [76]. Copyright 2024, Elsevier; (**h**) Rate capability of the TFEP-containing electrolyte system. Reproduced with permission [74]. Copyright 2024, Elsevier; (**i**) Relationship between desolvation energy and the size of the solvation sheath. Reproduced with permission [32]. Copyright 2024, Spring Nature; (**j**) Cycling stability of a graphite electrode at 6 C in 1.3 M LiFSI/FAN electrolyte. Reproduced with permission [32]. Copyright 2024, Spring Nature.

In addition to directly selecting solvents with intrinsically low desolvation energy, introducing weakly solvating co-solvents can also regulate the Li^+ solvation structure, thereby lowering the desolvation energy barrier. Chen et al. [76] employed ethyl bis(2,2,2-trifluoroethyl) phosphonate (TFEP) as a co-solvent for propylene carbonate (PC). The high degree of fluorination in TFEP significantly weakens its coordination ability with Li^+, allowing TFEP to co-occupy the primary Li^+ solvation sheath together with PF_6^- (Figure 12f,g). This unique solvation structure effectively reduces the Li^+ desolvation energy, leading to markedly improved rate capability and low-temperature performance of the battery (Figure 12h).

Furthermore, the use of small-molecule solvents with specialized transport mechanisms can further optimize charge-transfer kinetics. Fan et al. [32] adopted fluoroacetonitrile (FAN) as the electrolyte solvent, which exhibits low solvation energy, a low liquid-phase Li^+ diffusion energy barrier, and a small solvation-shell size (Figure 12i). In an ideal dilute solution, the transport index (TI) approaches 0, and Li^+ transport follows a vehicle mechanism. In solid-state electrolytes, TI ≈ 1, where Li^+ migrates via structural diffusion. However, in electrolytes with ligand-channel-assisted transport mechanisms, TI can approach 0.5, thereby overcoming the limitations of conventional transport modes. Consequently, the 1.3 M LiFSI/FAN electrolyte system enables stable cycling at high rates (≥6 C) under both room-temperature and elevated-temperature conditions (Figure 12j).

5. Fast-Charging Electrode Architectures

To achieve fast-charging capability, electrode structures should ideally combine high porosity and low tortuosity. However, high porosity inevitably reduces electrode compaction density, thereby sacrificing the volumetric energy density of the battery, which is an undesirable trade-off for practical applications. A more feasible solution is to design electrodes with a porosity gradient along the thickness direction. This strategy can be realized by tailoring the particle size distribution of graphite in different layers or by using differentiated slurry formulations. For example, in the top layer of the electrode (near the separator), a binder with lower compaction density can be used to reduce particle-particle contact and maintain higher porosity, thereby facilitating electrolyte infiltration and Li^+ transport. In contrast, the bottom layer (near the current collector) can employ a high-compaction binder, which strengthens particle bonding and forms a denser structure with lower porosity, ensuring high volumetric energy density and mechanical stability (Figure 13a). Based on this concept, Wu et al. [29] developed a three-layer porosity-gradient electrode, in which the porosity reaches 35% in the top layer and decreases to 15% in the bottom layer (Figure 13b). Compared with a control electrode with uniform porosity (25%), this gradient electrode exhibited superior rate capability and cycling stability (Figure 13c). Moreover, no abrupt voltage drop caused by lithium plating was observed during high-rate charging, indicating improved electrode kinetics and enhanced safety under fast-charging conditions.

Reducing electrode tortuosity is another key strategy for enhancing fast-charging performance, as it shortens the Li^+ transport pathways within the porous electrode. For example, laser drilling can create ion transport channels perpendicular to the current collector on the graphite anode surface (Figure 13d) [29,38,39]. This architecture significantly reduces the macroscopic tortuosity of the electrode, decreasing the constant-voltage charging time required for full lithiation of the graphite electrode and enabling stable fast charging at 6 C. Compared with high-tortuosity electrodes, the laser-drilled electrode exhibits negligible lithium plating at high rates. Another effective approach for reducing tortuosity is magnetically induced orientation [37]. Studart et al. [77] introduced superparamagnetic nanoparticles into the electrode slurry, enabling graphite platelets to align in an ordered manner perpendicular to the current collector under an external magnetic field (Figure 13e). This alignment reduced the electrode tortuosity by approximately fourfold. The resulting graphite electrode exhibited a threefold increase in capacity at 2 C (Figure 13f), clearly demonstrating the significant role of structural orientation in optimizing ion transport kinetics for fast-charging electrodes.

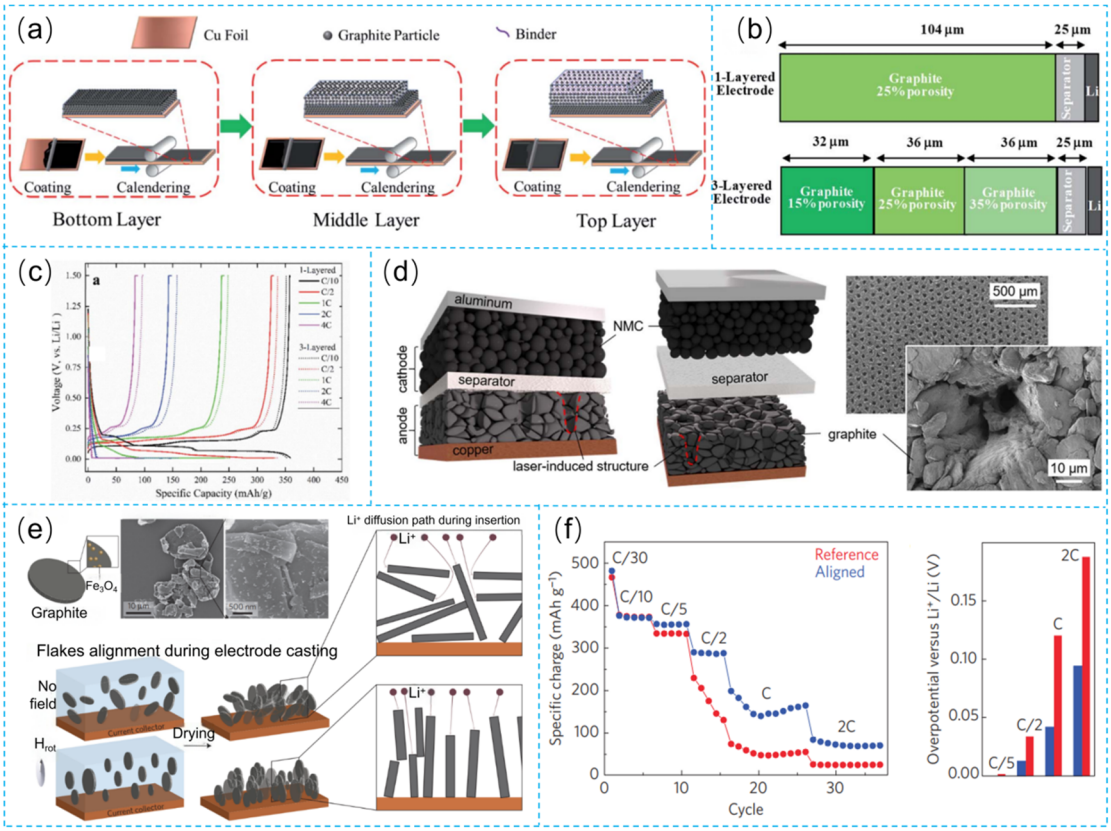

Figure 13. Design strategies for low-tortuosity electrode architectures and their electrochemical performance: (**a**) Schematic illustration of the fabrication process for a three-layer porosity-gradient electrode. Reproduced with permission [29]. Copyright 2022, Royal Society of Chemistry; (**b**) Structural diagram of the three-layer porosity-gradient electrode. Reproduced with permission [29]. Copyright 2022, Royal Society of Chemistry; (**c**) Comparison of the rate performance between gradient-porosity and uniform-porosity electrodes. Reproduced with permission [29]. Copyright 2022, Royal Society of Chemistry; (**d**) Schematic illustration of vertical ion-transport channels constructed via laser drilling. Reproduced with permission [38]. Copyright 2019, Electrochemical Society; (**e**) Schematic diagram of magnetically induced alignment of graphite platelets using superparamagnetic nanoparticles. Reproduced with permission [77]. Copyright 2016, Spring Nature; (**f**) Comparison of the rate capability between vertically aligned graphite electrodes and conventional electrodes. Reproduced with permission [77]. Copyright 2016, Spring Nature.

6. Conclusions and Outlook

Achieving extreme fast charging (XFC) in LIBs is critical for promoting the widespread adoption of EVs and alleviating public concerns over "charging anxiety". In this review, we systematically summarize recent advances and synergistic design strategies for realizing XFC across three key areas: graphite anodes, electrolytes, and electrode architectures. The core challenge of fast charging is lithium plating on graphite anodes under high-rate conditions, which originates from kinetic limitations (e.g., high Li^+ desolvation barriers and sluggish ion transport) as well as geometric/structural constraints (e.g., insufficient active sites and non-uniform polarization along the electrode thickness). To address these issues, a variety of multidimensional strategies have been proposed.

From the perspective of graphite anodes, current strategies primarily focus on two core principles: "increasing active-site availability" and "reducing interfacial resistance." Increasing active-site availability is achieved by creating additional Li^+ insertion pathways through approaches such as alkaline etching to generate porous structures, edge functionalization, and heterostructure construction, thereby increasing the density of surface active sites and redistributing local current to mitigate polarization. In contrast, reducing interfacial resistance targets the rate-determining desolvation step, typically by constructing artificial SEI layers enriched with functional groups (e.g., ether oxygen or phosphate groups) or low-work-function components (e.g., Li_3P). These modifications weaken the interaction between Li^+ and solvent molecules, thereby accelerating interfacial charge-transfer kinetics.

In electrolyte design, the research focus has shifted from maximizing ionic conductivity alone to the synergistic optimization of Li^+ transport efficiency and interfacial reaction kinetics. Representative strategies include: (1) introducing low-viscosity co-solvents and highly dissociative lithium salts (e.g., LiFSI) to enhance ionic conductivity; (2) employing weakly coordinating solvents or localized high-concentration electrolyte

(LHCE) structures to increase the Li^+ diffusion coefficient; (3) utilizing bulky anions, polyanionic electrolytes, or high-concentration strategies to significantly raise the Li^+ transference number (t_+) and suppress concentration polarization; and (4) developing low-desolvation-energy solvents such as ethers and fluorinated nitriles to lower the interfacial reaction barrier. An ideal fast-charging electrolyte must strike an optimal balance among these often mutually constrained properties.

With respect to electrode architectures, studies have advanced beyond traditional homogeneous porous electrodes toward engineered ion-transport networks. Porosity gradient design, with higher porosity near the separator and denser regions near the current collector, enables fast Li^+ transport while maintaining sufficient electrode compaction density. Moreover, advanced fabrication techniques such as laser structuring and magnetically induced assembly produce low-tortuosity or vertically aligned electrode structures, which act as ion highways to shorten Li^+ diffusion paths and ensure uniform reaction distribution across the electrode thickness under high-rate conditions.

When considering practical application conditions that demand a simultaneous balance of energy density, cycle life, safety, and cost, the strategies most relevant for XFC are those that directly target the rate-limiting desolvation step and ensure uniform ion transport, without compromising other performance metrics. Specifically: (i) constructing functional-group-enriched artificial SEIs on graphite to lower the desolvation barrier while maintaining interfacial stability; (ii) adopting weakly solvating or localized high-concentration electrolytes that achieve high Li^+ transference numbers and low desolvation energies, thereby suppressing concentration polarization and lithium plating; and (iii) implementing low-tortuosity or gradient-porosity electrode architectures that ensure rapid and homogeneous Li^+ flux distribution across the electrode thickness. Crucially, the compatibility and synergistic integration of these anode-electrolyte-electrode strategies in a full-cell configuration, rather than isolated optimization, determines their practical relevance. Although remarkable progress has been made in each of these individual fields, realizing system-level XFC under practical conditions remains a substantial challenge. Future efforts should focus on:

(1) Multi-objective collaborative optimization and system-level integration. Enhancing fast-charging performance must not come at the expense of energy density, cycle life, safety, or cost. Future efforts should shift from single-performance optimization to multi-objective collaborative design. For example, developing an ideal electrolyte that simultaneously exhibits a high Li^+ transference number and high ionic conductivity, designing electrode architectures compatible with both fast charging and high areal capacity, and exploring the compatibility and synergistic effects of various modification strategies in full-cell configurations.

(2) Mechanism deepening and quantitative modeling. The effectiveness of many current strategies still lacks atomistic- or molecular-scale mechanistic support and quantitative models. Future work should combine advanced operando characterization techniques with theoretical calculations to reveal the microscopic mechanisms of fast-charging and degradation processes (e.g., desolvation, SEI evolution, lithium deposition) at the atomic/molecular level. Establishing quantitative structure-property relationships from intrinsic material characteristics to macroscopic battery performance will provide precise guidance for the rational design of materials.

(3) Exploration of emerging materials and innovative technologies. While continuing to optimize graphite anodes, attention should also be directed toward more promising anode materials (e.g., hard carbon, Si/C composites) and new electrolyte systems based on novel lithium salts or solid-state/semi-solid electrolytes. At the same time, future efforts should explore the deep integration of smart charging protocols (e.g., pulse charging and self-heating strategies) with advanced battery management systems, aiming to achieve breakthroughs through the synergistic coupling of electrochemistry and thermal management.

(4) Degradation mechanisms and life management. Battery degradation under XFC conditions (e.g., the accumulation and evolution of lithium plating, degradation of high-voltage cathodes, and continuous electrolyte consumption) is far more complex than that observed under conventional cycling. Long-term aging studies specifically targeting XFC conditions are essential to establish accurate lifetime prediction models and to develop corresponding mitigation or recovery strategies (e.g., algorithm-based reversal of minor lithium plating). Such efforts are critical for ensuring the safety and reliability of batteries throughout their entire fast-charging lifecycle.

In summary, the development of XFC LIBs represents a complex systems-engineering challenge, the realization of which depends on the deep integration and comprehensive innovation across materials, devices, thermal management, and system-level control. Through sustained interdisciplinary efforts and close collaboration between academia and industry, the vision of charging as convenient as refueling can ultimately be realized, laying a solid foundation for transportation electrification and sustainable energy development.

Author Contributions

Q.D.: methodology, investigation, writing—original draft preparation, visualization. H.L.: conceptualization, writing—review and editing. X.A.: conceptualization, supervision, project administration, writing—review and editing. All authors have read and agreed to the published version of the manuscript.

Funding

This research received no external funding.

Institutional Review Board Statement

Not applicable.

Informed Consent Statement

Not applicable.

Data Availability Statement

No new data were generated or analyzed in support of this review. All data discussed or cited in this manuscript are available from the original publications referenced in the reference list.

Conflicts of Interest

The authors declare no conflict of interest.

Use of AI and AI-Assisted Technologies

No AI tools were utilized for this paper.

References

1. Fachrizal, R.; Qian, K.; Lindberg, O.; et al. Urban-scale energy matching optimization with smart EV charging and V2G in a net-zero energy city powered by wind and solar energy. *eTransportation* **2024**, *20*, 100314.
2. Yu, X.; Lin, C.; Xie, P.; et al. Electric-thermal collaborative control and multimode energy flow analysis of fuel cell hybrid electric vehicles in low-temperature regions. *eTransportation* **2024**, *21*, 100341.
3. Semieniuk, G.; Taylor, L.; Rezai, A.; et al. Plausible energy demand patterns in a growing global economy with climate policy. *Nat. Clim. Change* **2021**, *11*, 313–318.
4. Deutch, J. Decoupling economic growth and carbon emissions. *Joule* **2017**, *1*, 3–5.
5. Dunn, B.; Kamath, H.; Tarascon, J.-M. Electrical energy storage for the grid: A battery of choices. *Science* **2011**, *334*, 928–935.
6. Liu, Y.; Zhu, Y.; Cui, Y. Challenges and opportunities towards fast-charging battery materials. *Nat. Energy* **2019**, *4*, 540–550.
7. Yang, X.; Vishnugopi, B.S.; Mukherjee, P.P.; et al. Advancements in extreme fast charging to foster sustainable electrification. *One Earth* **2022**, *5*, 216–219.
8. Liu, T.; Yang, X.; Ge, S.; et al. Ultrafast charging of energy-dense lithium-ion batteries for urban air mobility. *eTransportation* **2021**, *7*, 100103.
9. Cai, W.; Yao, Y.; Zhu, G.; et al. A review on energy chemistry of fast-charging anodes. *Chem. Soc. Rev.* **2020**, *49*, 3806–3833.
10. Tomaszewska, A.; Chu, Z.; Feng, X.; et al. Lithium-ion battery fast charging: A review. *eTransportation* **2019**, *1*, 100011.
11. Weiss, M.; Ruess, R.; Kasnatscheew, J.; et al. Fast charging of lithium-ion batteries: A review of materials aspects. *Adv. Energy Mater.* **2021**, *11*, 2101126.
12. Finegan, D.P.; Quinn, A.; Wragg, D.S.; et al. Spatial dynamics of lithiation and lithium plating during high-rate operation of graphite electrodes. *Energy Environ. Sci.* **2020**, *13*, 2570–2584.
13. Adam, A.; Wandt, J.; Knobbe, E.; et al. Fast-charging of automotive lithium-ion cells: In-situ lithium-plating detection and comparison of different cell designs. *J. Electrochem. Soc.* **2020**, *167*, 130503.
14. Wang, G.; Bi, Z.; Zhang, A.; et al. High-voltage and fast-charging lithium cobalt oxide cathodes: From key challenges and strategies to future perspectives. *Engineering* **2024**, *37*, 105–127.
15. Ding, X.; Zhou, Q.; Li, X.; et al. Fast-charging anodes for lithium ion batteries: Progress and challenges. *Chem. Commun.* **2024**, *60*, 2472–2488.
16. Logan, E.R.; Dahn, J.R. Electrolyte design for fast-charging Li-ion batteries. *Trends Chem.* **2020**, *2*, 354–366.
17. Schmuch, R.; Wagner, R.; Hörpel, G.; et al. Performance and cost of materials for lithium-based rechargeable automotive

batteries. *Nat. Energy* **2018**, *3*, 267–278.
18. Jiang, M.; Li, D.; Li, Z.; et al. Advances in battery state estimation of battery management system in electric vehicles. *J. Power Sources* **2024**, *612*, 234781.
19. Ruan, D.; Chen, S.; Guo, J.; et al. Molecularly aligned electron channels for ultrafast-charging practical lithium-metal batteries. *Nat. Energy* **2026**, *11*, 425–435.
20. Wang, Q.; Yao, Z.; Wang, J.; et al. Chemical short-range disorder in lithium oxide cathodes. *Nature* **2024**, *629*, 341–347.
21. Zhao, W.; Zhao, C.; Wu, H.; et al. Progress, challenge and perspective of graphite-based anode materials for lithium batteries: A review. *J. Energy Storage* **2024**, *81*, 110409.
22. Zhang, Y.; Wu, B.; Mu, G.; et al. Recent progress and perspectives on silicon anode: Synthesis and prelithiation for libs energy storage. *J. Energy Chem.* **2022**, *64*, 615–650.
23. Manthiram, A.; Goodenough, J.B. Layered lithium cobalt oxide cathodes. *Nat. Energy* **2021**, *6*, 323.
24. Yuan, K.; Lin, Y.; Li, X.; et al. High-safety anode materials for advanced lithium-ion batteries. *Energy Environ. Mater.* **2024**, *7*, e12759.
25. Liu, Y.; Zhao, C.; Du, J.; et al. Research progresses of liquid electrolytes in lithium-ion batteries. *Small* **2023**, *19*, 2205315.
26. Zhu, G.; Zhao, C.; Huang, J.; et al. Fast charging lithium batteries: Recent progress and future prospects. *Small* **2019**, *15*, 1805389.
27. Jeong, Y.T.; Shin, H.R.; Lee, J.; et al. Insight into pulse-charging for lithium plating-free fast-charging lithium-ion batteries. *Electrochim. Acta* **2023**, *462*, 142761.
28. Mao, C.; Ruther, R.E.; Li, J.; et al. Identifying the limiting electrode in lithium ion batteries for extreme fast charging. *Electrochem. Commun.* **2018**, *97*, 37–41.
29. Yang, J.; Li, Y.; Mijailovic, A.; et al. Gradient porosity electrodes for fast charging lithium-ion batteries. *J. Mater. Chem. A* **2022**, *10*, 12114–12124.
30. Yao, Z.X.; Xu, T.Q.; Zhang, R.M.; et al. X bp index as a predictive tool for fast-charging performance of artificial graphite anodes in lithium-ion batteries. *J. Mater. Chem. A* **2025**, *13*, 33147–33159.
31. Sun, C.; Ji, X.; Weng, S.; et al. 50c fast-charge li-ion batteries using a graphite anode. *Adv. Mater.* **2022**, *34*, 2206020.
32. Lu, D.; Li, R.; Rahman, M.M.; et al. Ligand-channel-enabled ultrafast Li-ion conduction. *Nature* **2024**, *627*, 101–107.
33. Sheng, Y.; Yue, X.; Hao, W.; et al. Heterojunction-coated graphite anode enables fast charging via built-in electric field-regulated interfacial Li-ion transport. *ACS Energy Lett.* **2025**, *10*, 5075–5083.
34. Buyting, S.; Schönhoff, M. Enhanced li transference in polymer electrolytes: Why anion size affects cation mobility. *ACS Appl. Polym. Mater.* **2025**, *7*, 8432–8444.
35. Lu, Y.; Wang, K.; Liu, Y. Gel polymer electrolytes based on single-ion-conducting polyelectrolyte (sicp) and sicp-functionalized carbon nanotubes. *Chem. Commun.* **2025**, *61*, 12936–12939.
36. Son, S.B.; Zhu, Q.J.; Garcia, J.; et al. Impact of the $LiPF_6$ concentration on the interfacial charge transfer and fast-charging capabilities of lithium-ion batteries. *J. Electrochem. Soc.* **2025**, *172*, 080532.
37. Yang, K.; Jiang, Y.; Huang, C. Fabrication of vertically aligned porous graphite anodes via magnetic field-assisted freezing casting for high-performance lithium-ion batteries. *Int. J. Electrochem. Sci.* **2023**, *18*, 100348.
38. Habedank, J.B.; Kriegler, J.; Zaeh, M.F. Enhanced fast charging and reduced lithium-plating by laser-structured anodes for lithium-ion batteries. *J. Electrochem. Soc.* **2019**, *166*, A3940.
39. Vennam, G.; Singh, A.; Dunlop, A.R.; et al. Fast-charging lithium-ion batteries: Synergy of carbon nanotubes and laser ablation. *J. Power Sources* **2025**, *636*, 236566.
40. Ali, A.O.; Abdelrehim, O.; Saafan, M.M.; et al. Comprehensive review of battery management systems for electric vehicles: Thermal management, charging strategies, and emerging technologies. *J. Power Sources* **2025**, *658*, 238269.
41. Fekri, Y.; Heyhat, M.M.; Jedari Salehzadeh, F.; et al. A review of thermal management systems for extreme fast charging Li-ion batteries. *Appl. Therm. Eng.* **2025**, *279*, 127870.
42. Yi, X.; Shi, L.; Chen, X.; et al. A decoupled two-stage optimization framework for the multi-objective coordination of charging efficiency and battery health. *Energies* **2025**, *18*, 5180.
43. Cheng, H.; Ma, Z.; Kumar, P.; et al. High voltage electrolyte design mediated by advanced solvation chemistry toward high energy density and fast charging lithium-ion batteries. *Adv. Energy Mater.* **2024**, *14*, 2304321.
44. Li, Z.; Wang, L.; Huang, X.; et al. Lithium bis(trifluoromethanesulfonyl)imide (LiTFSI): A prominent lithium salt in lithium-ion battery electrolytes—Fundamentals, progress, and future perspectives. *Adv. Funct. Mater.* **2024**, *34*, 2408319.
45. Liu, Y.; Shi, H.; Wu, Z. Recent status, key strategies and challenging perspectives of fast-charging graphite anodes for lithium-ion batteries. *Energy Environ. Sci.* **2023**, *16*, 4834–4871.
46. Zhong, C.; Weng, S.; Wang, Z.; et al. Kinetic limits and enhancement of graphite anode for fast-charging lithium-ion batteries. *Nano Energy* **2023**, *117*, 108894.
47. Cheng, Q.; Yuge, R.; Nakahara, K.; et al. Koh etched graphite for fast chargeable lithium-ion batteries. *J. Power Sources* **2015**, *284*, 258–263.

48. Kim, N.; Chae, S.; Ma, J.; et al. Fast-charging high-energy lithium-ion batteries via implantation of amorphous silicon nanolayer in edge-plane activated graphite anodes. *Nat. Commun.* **2017**, *8*, 812.
49. Hu, J.; Zhu, Y.; Zeng, X.; et al. Fast charging performance of graphite etched under mild conditions and promotion mechanism. *J. Power Sources* **2024**, *622*, 235337.
50. Park, J.; Lee, M.; Jeon, I.; et al. Edge-exfoliated graphites for facile kinetics of delithiation. *ACS Nano* **2012**, *6*, 10770–10775.
51. Du, P.; Zhang, B.; Cao, L.; et al. Designed graphite with an activated edge for fast-charging lithium-ion storage properties. *Chem. Commun.* **2022**, *58*, 7372–7375.
52. Cai, W.; Yan, C.; Yao, Y.; et al. Rapid lithium diffusion in order@disorder pathways for fast-charging graphite anodes. *Small Struct.* **2020**, *1*, 2000010.
53. Du, P.; Fan, X.; Zhang, B.; et al. The lithiophobic-to-lithiophilic transition on the graphite towards ultrafast-charging and long-cycling lithium-ion batteries. *Energy Storage Mater.* **2022**, *50*, 648–657.
54. Li, F.; Wu, Y.; Chou, J.; et al. A mechanically robust and highly ion-conductive polymer-blend coating for high-power and long-life lithium-ion battery anodes. *Adv. Mater.* **2015**, *27*, 130–137.
55. Song, C.; Zhao, J.; Ma, S.; et al. Ordered lithium-ion conductive interphase with gradient desolvation effects for fast-charging lithium metal batteries. *ACS Energy Lett.* **2023**, *8*, 3404–3411.
56. Wang, C.; Xie, Y.; Huang, Y.; et al. Li_3PO_4-enriched sei on graphite anode boosts Li^+ de-solvation enabling fast-charging and low-temperature lithium-ion batteries. *Angew. Chem. Int. Ed.* **2024**, *63*, e202402301.
57. Tu, S.; Zhang, B.; Zhang, Y.; et al. Fast-charging capability of graphite-based lithium-ion batteries enabled by Li_3P-based crystalline solid–electrolyte interphase. *Nat. Energy* **2023**, *8*, 1365–1374.
58. Wang, J.; Zhang, J.; Wu, J.; et al. Interfacial "single-atom-in-defects" catalysts accelerating Li^+ desolvation kinetics for long-lifespan lithium-metal batteries. *Adv. Mater.* **2023**, *35*, 2302828.
59. Zhang, S.S. Reformulation of electrolyte for enhanced fast-charge capability of Li-ion battery. *J. Electrochem. Soc.* **2020**, *167*, 060527.
60. Wu, X.; Liu, T.; Bai, Y.; et al. Effects of solvent formulations in electrolytes on fast charging of Li-ion cells. *Electrochim. Acta* **2020**, *353*, 136453.
61. Logan, E.R.; Hall, D.S.; Cormier, M.M.E.; et al. Ester-based electrolytes for fast charging of energy dense lithium-ion batteries. *J. Phys. Chem. C* **2020**, *124*, 12269–12280.
62. Zou, Y.; Cao, Z.; Zhang, J.; et al. Interfacial model deciphering high-voltage electrolytes for high energy density, high safety, and fast-charging lithium-ion batteries. *Adv. Mater.* **2021**, *33*, 2102964.
63. Du, Z.; Wood, D.L.; Belharouak, I. Enabling fast charging of high energy density Li-ion cells with high lithium ion transport electrolytes. *Electrochem. Commun.* **2019**, *103*, 109–113.
64. Zhang, L.; Chai, L.; Zhang, L.; et al. Synergistic effect between lithium bis(fluorosulfonyl)imide (LiTFSI) and lithium bis-oxalato borate (LiBOB) salts in $LiPF_6$-based electrolyte for high-performance li-ion batteries. *Electrochim. Acta* **2014**, *127*, 39–44.
65. Hayamizu, K.; Aihara, Y.; Arai, S.; et al. Pulse-gradient spin-echo 1H, 7Li, and 19F nmr diffusion and ionic conductivity measurements of 14 organic electrolytes containing $LiN(SO_2CF_3)_2$. *J. Phys. Chem. B* **1999**, *103*, 519–524.
66. Stewart, S.G.; Newman, J. The use of uv/vis absorption to measure diffusion coefficients in $LiPF_6$ electrolytic solutions. *J. Electrochem. Soc.* **2008**, *155*, F13.
67. Hayamizu, K. Temperature dependence of self-diffusion coefficients of ions and solvents in ethylene carbonate, propylene carbonate, and diethyl carbonate single solutions and ethylene carbonate + diethyl carbonate binary solutions of $lipf_6$ studied by nmr. *J. Chem. Eng. Data* **2012**, *57*, 2012–2017.
68. Ren, X.; Chen, S.; Lee, H.; et al. Localized high-concentration sulfone electrolytes for high-efficiency lithium-metal batteries. *Chem* **2018**, *4*, 1877–1892.
69. Diederichsen, K.M.; McShane, E.J.; McCloskey, B.D. Promising routes to a high Li^+ transference number electrolyte for lithium ion batteries. *ACS Energy Lett.* **2017**, *2*, 2563–2575.
70. Armand, M.; Johansson, P.; Bukowska, M.; et al. Review—Development of hückel type anions: From molecular modeling to industrial commercialization. A success story. *J. Electrochem. Soc.* **2020**, *167*, 070562.
71. Popovic, J.; Höfler, D.; Melchior, J.P.; et al. High lithium transference number electrolytes containing tetratriflylpropene's lithium salt. *J. Phys. Chem. Lett.* **2018**, *9*, 5116–5120.
72. Zhou, P.; Zhang, X.; Xiang, Y.; et al. Strategies to enhance Li^+ transference number in liquid electrolytes for better lithium batteries. *Nano Res.* **2023**, *16*, 8055–8071.
73. Buss, H.G.; Chan, S.Y.; Lynd, N.A.; et al. Nonaqueous polyelectrolyte solutions as liquid electrolytes with high lithium ion transference number and conductivity. *ACS Energy Lett.* **2017**, *2*, 481–487.
74. Fong, K.D.; Self, J.; Diederichsen, K.M.; et al. Ion transport and the true transference number in nonaqueous polyelectrolyte solutions for lithium ion batteries. *ACS Cent. Sci.* **2019**, *5*, 1250–1260.
75. Nakanishi, A.; Ueno, K.; Watanabe, D.; et al. Sulfolane-based highly concentrated electrolytes of lithium

bis(trifluoromethanesulfonyl)amide: Ionic transport, Li-ion coordination, and Li–S battery performance. *J. Phys. Chem. C* **2019**, *123*, 14229–14238.

76. Chen, L.; Wang, J.; Chen, M.; et al. "Dragging effect" induced fast desolvation kinetics and −50 °C workable high-safe lithium batteries. *Energy Storage Mater.* **2024**, *65*, 103098.
77. Billaud, J.; Bouville, F.; Magrini, T.; et al. Magnetically aligned graphite electrodes for high-rate performance Li-ion batteries. *Nat. Energy* **2016**, *1*, 16097.